Short-Term Voltage Stability Analysis for Power System with Single-Phase Motor

Load

By

Yan Ma

A Thesis Presented in Partial Fulfillment
of the Requirements for the Degree
Master of Science

Approved April 2012 by the
Graduate Supervisory Committee:

George G. Karady, Chair
Vijay Vittal
Raja Ayyanar

ARIZONA STATE UNIVERSITY

May 2012

ABSTRACT

Voltage stability is always a major concern in power system operation. Recently Fault Induced Delayed Voltage Recovery (FIDVR) has gained increased attention. It is widely believed that the motor-driven loads of high efficiency, low inertia air conditioners are one of the main causes of FIDVR events.

Simulation tools that assist power system operation and planning have been found insufficient to reproduce FIDVR events. This is because of their inaccurate load modeling of single-phase motor loads. Conventionally three-phase motor models have been used to represent the aggregation effect of single-phase motor load. However researchers have found that this modeling method is far from an accurate representation of single-phase induction motors.

In this work a simulation method is proposed to study the precise influence of single-phase motor load in context of FIDVR. The load, as seen the transmission bus, is replaced with a detailed distribution system. Each single-phase motor in the distribution system is represented by an equipment-level model for best accuracy. This is to enable the simulation to capture stalling effects of air conditioner compressor motors as they are related to FIDVR events.

The single phase motor models are compared against the traditional three phase aggregate approximation. Also different percentages of single-phase motor load are compared and analyzed.

Simulation result shows that proposed method is able to reproduce FIDVR events. This method also provides a reasonable estimation of the power system voltage stability under the contingencies.

ACKNOWLEDGEMENTS

TABLE OF CONTENTS

LIST OF TABLES

LIST OF FIGURES

NOMENCLATURE

AC   Alternating current

AGC   Automatic generation control

APS   Arizona Public Services

AVR   Automatic Voltage Regulator

DC   Direct current

DOE   Department of Energy

EPRI   Electric Power Research Institute

FIDVR   Fault Induced Delayed Voltage Recovery

GE   General Electric Company

IEEE   Institute of Electrical and Electronics Engineers

ISO   Independent System Operator

LMTF   Load Modeling Task Force

NERC   North American Electric Reliability Corporation

P   Active power

PES   Power and Energy Society

PSAT   Power System Analysis Toolbox

PSLF   Positive Sequence Load Flow Software

Q   Reactive power

RAC   Residential Air Conditioner

SCE   Southern California Edison

SEER   Seasonal Energy Efficiency Ratio

SVS   Static VAR Source

RPM   Revolutions Per Minute

TOL   Thermal Over Load

ULTC   Under Load Tap Changing

V   Voltage

WECC   Western Electricity Coordinating Council

Z   Impedance

ZIP   Constant impedance/current/power load

1PH   Single-phase

3PH   Three-phase

CHAPTER 1

INTRODUCTION

1.1   Background

Power systems have developed into one of the largest industries in the

world. Trends of growth have however led to limiting constraints of power system

operation [1]. One of the major concerns is power system stability. General

classifications are rotor angle (synchronous), frequency, and voltage stability [2]

[3].

Voltage stability is the ability of a power system to maintain steady

acceptable voltages at all buses under normal operation after being subjected to a

disturbance [1]. Voltage instability is the absence of voltage stability as it leads to

progressive voltage decrease or increase [3]. Voltage instability and voltage

collapse are sometimes synonymous.

1.2   Motivation

Load characteristics have a strong influence on power system voltage

stability. Since voltage instability is believed to be caused by the shortage of

reactive power, most voltage stability studies are concentrated on predicting the

load's reactive power and planning reactive power generation.

Induction motor loads have been found to be a major contributing factor to

voltage instability. When the applied voltage on the motor is reduced to a certain

level, as the result of a fault, the motor suddenly requires much more active and

reactive power. In the worst case, if the induction motors stalls, the motor

typically requires around five times more power than in steady state. The

increased power requirements lead to further depressed system voltage and consequently more induction motors may slow or stall. In this situation, either the system needs more time to recover or the system may experience voltage collapse.

Recently, there has been a growing concern about a short-term voltage instability issue termed Fault Induced Delayed Voltage Recovery (FIDVR). The cause of this phenomenon is believed to be motor-driven loads of Residential Air Conditioners (RAC).

According to the DOE 1980-2001 appliance report [4], about 55% of US households have central air-conditioners and about 23% US households have individual room units. With the significantly increasing demand for RACs, electric utilities are experiencing more FIDVR events.

Conventionally three-phase motor models have been utilized in simulation to represent the aggregation effect of all motor loads. However present power system simulation tools have been found insufficient to reproduce the FIDVR events. This is due to their inaccurate representation of the single-phase induction motor.

1.3   Research scope and objective

The objective of this work is to study the influence of the single-phase motor loads on the power system voltage stability problem. The specific tasks include:

- Develop a modeling method to accurately represent the behavior of single-phase induction motor load in power system simulation.

2

- Design and build in simulation a detailed distribution system with different percentage of single-phase motor load. Each single-phase motor will be represented with an equipment-level model.

- Create composite load models to represent the distribution systems. Each composite load model will be composed of a constant impedance load (static load), and a three-phase motor model (dynamic load) that represents the aggregation effect of all single-phase motor loads in the distribution system.

- Compare simulation results from the composite load model against the detailed distribution system while varying the percentage of motor load.

- Investigate the relationship between the percentages of single-phase motor load and their impact on voltage stability.

1.4   Thesis organization

This thesis includes seven chapters and is organized as follows.

Chapter 2 provides a brief literature review associated with voltage stability, such as the definition of voltage stability, voltage stability analysis methods, and the FIDVR phenomenon.

Chapter 3 reviews load modeling in power systems. A brief description is presented on categorization of loads and a variety of load modeling methods. Also models for three-phase and single-phase induction motors are presented.

Chapter 4 introduces characteristics of the RAC and explains why it is important to model RACs in power system simulation. A variety of RAC models

are also discussed. A literature survey is presented on current research in modeling RACs for power system simulation. Furthermore detailed load models are introduced for later use in simulation.

In *Chapter 5*, a method is proposed to study the precise influence of the RAC motors on the power system.

Chapter 6 presents the results and comparisons of various case studies.

Chapter 7 summarizes the contributions of this research and provides recommendations for future work.

CHAPTER 2

VOLTAGE STABILITY

Voltage stability has imposed more constraints to power system operation than the past. This is because current power systems are normally operating close to stability limits. Some large-scale blackouts are believed to have been caused by voltage instability.

2.1   What is voltage stability?

Generally, voltage stability is defined as the capability of power system to maintain acceptable voltage at all the buses in the system after being subjected to a disturbance from a given initial operating condition [1]. Voltage instability is the absence of the voltage stability and may result in a progressive unacceptable increase or decrease of voltage of some buses, thus causing load shed and voltage collapse [3].

Voltage collapse is a dynamic phenomenon usually characterized as a gradual voltage magnitude decrease and then a sharp accelerated drop after a few minutes. The fundamental cause of voltage collapse is the inability of the power system to meet its demand for reactive power [1]. A number of voltage collapse incidents [3][5][6] have been reported over the past years and are usually caused by the following major factors:

- The fast continuing increase of the load

- The insufficient reactive power support

- Long transmission line fault or malfunction of its protection

- Incorrect adjustment of the Under Load Tap Changer (ULTC)

- Poor coordination among control and protection devices

- Unfavorable load characteristics

- Long distance between generators and load

Although voltage magnitude will drop when voltage collapse occurs, a low voltage at the receiving end does not necessarily indicate a risk of voltage collapse [7] [8]. On the contrary, in some cases the bus voltage may drop (from heavy load) while the system is still in stable operation. In other cases voltage collapse may occur when the bus voltage is still within limits. Consequently, the study of voltage stability should take into account not only voltage magnitude, but also other system parameters such as phase angle, admittance matrix, load, and generator information.

2.2   Voltage stability categorization

Reference [1] and [3] categorize voltage stability in different aspects. Based on the scale of the disturbance, they are:

- Large-disturbance voltage stability. This classification deals with the capability of the power system to control voltages when subjected to a large disturbance such as loss of generation or transmission line fault.

- Small-disturbance voltage stability is related to the system's capability to maintain acceptable voltages when small perturbations occur. The small perturbations may be the changes in system load, the action of the system control, etc.

Voltage stability can also be categorized based on the time period.

- In long-term voltage stability, the range of time period may be a few minutes to 10's of minutes. This involves slower systems and equipment such as AGC, tap-changing transformers, and transformer saturation.

- Mid-term voltage stability is typically in the range of about 10 seconds to a few minutes. This type of voltage stability includes synchronizing power oscillation among machines and large voltage or frequency excursions.

- Short-term or transient voltage stability is usually studies in the scale below 10 seconds. This involves dynamics of fast acting load components such as induction motors, electronically controlled loads, and HVDC converters.

2.3   Voltage stability analysis methods

Generally voltage stability analysis can be classified as static or dynamic [9] [10]. Static analysis entails capturing snapshots of system conditions at an instant in time. This reduces overall system equations to purely algebraic.

Dynamic analysis utilizes time domain simulation and considers appropriate dynamic modeling to capture events that lead the system to voltage instability. The dynamic analysis methods include models of power system elements that have an influential impact on voltage instability [1].

Compared with static analysis, dynamic analysis provides more accurate representation of voltage instability. This is useful for detailed study of a specific system to test coordination, protection and for remedial measures. However,

7

dynamic simulations are more time-consuming than static. This constraint limits

the application of dynamic modeling in studying the bulk power system. In

contrast, static analysis is less computational intensive, and is able to determine

the voltage stability at selected snapshots. If used appropriately, the static method

is able to provide much insight into the nature of the problem and identify the key

contributing elements. Therefore, static analysis is widely utilized for analyzing

voltage stability of bulk power system. In some cases, researchers have combined

both static and dynamic analysis to exploit the advantages of each. Reference [11]

utilizes static analysis to identify the weak elements, and then models them in

more detail with dynamic analysis.

Voltage instability is essentially a nonlinear phenomenon, and it is usually

evaluated using bifurcation theory. Bifurcation theory is the mathematical study

of how and when the solutions to a system change as a result of parameter

changes. Bifurcation theory has the following characteristics when it is applied to

the analysis of voltage stability [5]:

- System parameters are assumed to change slowly.

- System instability occurs when a small change of system parameters
  cause qualitative changes.

- In a saddle-node bifurcation, the equilibrium disappears with small
  parameter change and consequently the system's voltage collapses
  dramatically.

2.4   Voltage stability indices

Voltage stability indices have been developed to detect proximity of a

system to voltage collapse. Voltage stability indices can be used on-line or off-line to assist the operators in determining how close a system is to voltage instability and what is the mechanism driving the instability. A good index should have the following characteristics [9] [12]:

- Accurate

- Linear

- Fast

- Providing sufficient information

- Simple

Past research on static analysis of voltage stability are generally divided into two categories.

2.4.1   Security margin

One category entails finding a security margin and the distance the current equilibrium point is from the instability region. The security margin of a power system depends on the system's load margin under normal and contingency situations. The load margin of the system is defined as the amount of additional load that would cause a voltage collapse for a particular operating equilibrium [5]. The following indices belong to this category [1]:

- Voltage stability index based on V-P characteristics of the system. System V-P characteristics are the result of several power flow simulations for different load level at a given power factor. However V-P characteristics of the system may not predict voltage collapse correctly because of changing power factor.

9

- Voltage stability index based on V-Q characteristics of the system. The Q-V characteristics of the system show the sensitivity of a bus voltage to reactive power. The bus being analyzed for its VQ curve is converted to a PV bus without reactive power limits. The calculation of VQ curves is time-consuming, and the bus reactive power injection or absorption is limited in reality. Therefore the Q-V characteristics of the system are useful but not commonly used for estimating voltage stability of bulk system.

- Voltage stability index based upon the minimal load increment. As presented in [13], the purpose of this method is to find the minimal active and reactive power increments that may cause voltage collapse. The success of this method depends on the initial direction chosen for loading.

- Voltage stability index based on reactive power limit. This was developed based on the theory that the fundamental cause of voltage collapse is the incapability of a power system to meet its demand for reactive power[1].

2.4.2   Voltage collapse indicator

The other category of static analysis is based upon finding a voltage collapse indicator for which an emergency threshold may be set. Several types are listed here:

- The V-Q sensitivity analysis [14][15] method assumes that P is constant ($\Delta P=0$) at each operating point, and the relationship between

ΔQ and ΔV is capable of assessing the voltage stability. This method only works well for small change of operation state.

- The Q-V modal analysis method [16] was developed from Q-V sensitivity analysis. The method computes the eigenvalue and eigenvector matrix of the reduced Q-V Jacobian marix. Besides providing estimation of voltage stability, the Q-V modal analysis also provides information regarding the mechanism of instability. Several techniques [1][17][18] have been developed to provide fast Q-V model analysis.

- Singular value decomposition analysis [17][19][20][21] was derived from a linear power flow model based upon the system's Jacobian matrix. The method evaluates the distance of the current Jacobian matrix to becoming singular. This method not only predicts voltage collapse, but also provides useful information for selecting remedial control measures.

- Voltage Collapse Proximity Indicator (VCPI) [22] assumes that near maximum loading conditions, small increase in load would require a significant amount of reactive power due to large line losses. Two indicators, VCPIp and VCPIq, are used to assess the sensitivity between total change in generator reactive power and the change in active and reactive load. The buses with high VCPIp value are the most effective location for load shielding, and the buses with high

VCPIq value are the most effective location for reactive power compensation.

- Voltage Instability Proximity Index (VIPI) [23][24][25]. This method estimates the voltage instability margin by calculating the angle θ between the specific vector and the critical vector.

- The steady state voltage stability indicator [26] method calculates indicators for voltage stability of each load bus by solving load flow. It is able to predict voltage collapse without actually computing load flows for extreme loading conditions. The stability indicator L is easy to be calculated with a simple formula and its range is from 0 to 1. The smaller the L, the more stable the system. This method is widely utilized.

- Some local indicators are for critical parts (nodes or area) of the system [27][28]. Sometimes system stability only depends on load change of critical parts (nodes or area). This type of indicator can be used for on-line voltage stability analysis because of its fast computation speed.

2.5   FIDVR phenomenon

The FIDVR event is a short-term voltage stability phenomenon. FIDVR occurs after a system fault. Once the fault has been cleared, the system voltage remains at the significant low level for several seconds or longer. In [29], NERC Transmission Issues Subcommittee defined the FIDVR as a voltage condition that is initiated by a fault and characterized as:

- Induction motors stall

- The voltage is initially recovered to less than 90% of pre-contingency voltage after the fault has been cleared

- The voltage is slowly (more than 2 seconds) restored to the expected post-contingency steady state voltage levels

FIDVR phenomenon is not new, but most FIDVR events were recently observed and reported. In [30], Southern California Edison (SCE) Company described an FIDVR event that occurred in June 1990. This phenomenon followed fault clearing in the transmission system and involved 1000 square miles. This paper also mentions the FIDVR observed by Sacramento Municipal Utility District in August 1990 and by Memphis in 1987. There have been at least eight FIDVR events in Southeast Florida between 1985 and 1995 [31]. Reference [32] presents FIDVR events following a multiple contingency fault and breaker failure at two 230 kV substations in Metro Atlanta. Reference [33] describes an FIDVR even in 2003 that was initiated by a three-phase fault on the Arizona Public Services (APS) system. Other FIDVR events are discussed in [34]. These reports and papers indicate FIDVR is mainly associated with high concentrations of induction motor loads.

The motors that have contributed to recent FIDVR events are low inertia, high efficiency, single phase induction motors of Residential Air Conditioners (RAC). These machines are easy to stall and draw a very high current during stall state. If the system does not have enough active and reactive power support, the high power demand of stalled RACs will further deteriorate voltage stability

causing more induction motors to stall thus leading to voltage collapse.

Many methods have been proposed to solve FIDVR problem. They can be categorized as follows [34]:

- The customer-level solution entails adjusting the RAC protection devices to help the RACs overcome or disconnect from the voltage transient instability. Although RAC manufacturers are hesitant to modify their standards.

- The system solution includes reducing fault clearing time, utilizing reactive power compensation devices, limiting load with adverse influence, improving system protection, etc. However since this method does not necessarily prevent RAC stalling, FIDVR events can be reduced but not eliminated.

At present, the controlled reactive power support at the grid level is believed to an efficient method. Also in practice utilities have installed generation and Static VAR Compensators (SVC) to alleviate FIDVR events.

CHAPTER 3

POWER SYSTEM LOAD MODELING

Many techniques and tools have been developed to simulate power system operation. One of the determining factors for accuracy is correct representation of power system equipment. However load is the most difficult aspect to model because of its great diversity.

For appropriate power system planning and operation, detailed load models are needed. In this chapter, modeling and analysis of electrical motor loads are introduced. In particular single and three-phase induction motors are described in detail.

3.1   Overview

As defined in [3], if the load voltages reach post-disturbance equilibrium after a disturbance, the power system is under stable operation. This definition also implies that for a stable power system, power generation should match consumption. Therefore loads have a strong influence on the system stability.

The power system load is comprised of many different devices such as motors, ovens, heaters, lamps, refrigerators, furnaces, and so on. These loads change with time, weather, economy, and other factors [1]. Also these millions of devices usually have their own special characteristics. Consequently it is not easy to build a load model to represent a practical load.

In most of power system simulations the load is considered an equivalent load that represents an aggregate effect of many individual devices [5]. For most power system studies, the aggregation is at a substation or distribution point.

3.2   Load model category

Traditionally load models are divided into two categories: static and dynamic. A composite load model includes both static and dynamic elements to represent the aggregate characteristics of various loads.

3.2.1   Static load model

The static model of the load provides the active and reactive power needed at any time based on simultaneously applied voltage and frequency. Static load models are capable of representing static load components such as resistive and reactive elements. They can also be used as a low frequency approximation of dynamic loads such as induction motors. However the static load model is not able to represent the transient response of dynamic loads [35].

Traditionally there are three types of static load models: voltage dependent, constant impedance/current/power (ZIP), and frequency dependent. The active and reactive power component of the static load model are always treated separately [1] [35].

Voltage dependent load is represented as an exponential model:

$$P = P_0 \left(\frac{V}{V_0}\right)^a \qquad\qquad (3.1)$$

$$Q = Q_0 \left(\frac{V}{V_0}\right)^b \qquad\qquad (3.2)$$

where

V_0 - Initial load bus voltage

V - Voltage applied on the load

P_0 and Q_0 - Load active and reactive components when the applied voltage is V_0

16

P and *Q*   - Load active and reactive components when the applied voltage is *V*

a and *b*   - Exponential parameters

When *a* and *b* are equal to 0, 1, and 2, the model represents the constant power, constant current, and constant impedance load respectively. For a common composite system *a* falls in the range of 0.5 to 1.8 and *b* is in the range of 1.5 to 6.

The *ZIP load model* is a polynomial that is composed of constant impedance, constant current, and constant power elements. The ZIP load is expressed as

$$P = P_0 \left(p_1 \left(\frac{V}{V_0} \right)^2 + p_2 \left(\frac{V}{V_0} \right) + p_3 \right) \tag{3.3}$$

$$Q = Q_0 \left(q_1 \left(\frac{V}{V_0} \right)^2 + q_2 \left(\frac{V}{V_0} \right) + q_3 \right) \tag{3.4}$$

where V_0, V, P_0, Q_0, P, and Q represent the same parameters as shown in the voltage dependent model. Other parameters are as follows:

p_1, p_2, and p_3 - Coefficients for defining the proportion of conductance, active current, and active power components

q_1, q_2, and q_3 - Coefficients for defining the proportion of susceptance, reactive current, and reactive power components

The *Frequency dependent load model* is represented by multiplying a frequency dependent factor with the voltage dependent model as shown in Equation (3.5) and (3.6) or with the ZIP model as shown in Equation (3.7) and (3.8),

$$P = \left[P_0 \left(\frac{V}{V_0} \right)^a \right] \left[1 + K_{pf}(f - f_0) \right] \tag{3.5}$$

$$Q = \left[Q_0 \left(\frac{V}{V_0} \right)^b \right] \left[1 + K_{qf}(f - f_0) \right] \tag{3.6}$$

$$P = \left[P_0 \left(p_1 \left(\frac{V}{V_0} \right)^2 + p_2 \left(\frac{V}{V_0} \right) + p_3 \right) \right] \left[1 + K_{pf}(f - f_0) \right] \tag{3.7}$$

$$Q = \left[Q_0 \left(q_1 \left(\frac{V}{V_0} \right)^2 + q_2 \left(\frac{V}{V_0} \right) + q_3 \right) \right] \left[1 + K_{qf}(f - f_0) \right] \tag{3.8}$$

where, V_0, V, P_0, Q_0, P, and Q represent the same parameters as shown in the voltage dependent model. Other parameters are as follows:

f_0 - Initial bus frequency

f - Applied bus frequency

K_{pf} - Parameters ranging from 0 to 3.0

K_{qf} - Parameters ranging from -2.0 to 0

3.2.2   Dynamic load model

A dynamic load model is a differential equation that gives the active and reactive power at any time based on instantaneous and past applied voltage and frequency [35]. Typical devices and controls that contribute to load dynamics are:

- Induction motor

- Protection system

- Discharge lamp

- Load with thermostatic control

- Other devices with dynamics such as HVDC converter, transformer ULTC, voltage regulator, and so on

Modeling dynamic load is much more difficult than modeling static load but is essential for short term voltage stability studies.

3.2.3   Composite load model

To represent aggregate characteristics of various load components, it is necessary to consider composite load models that take into account both static and dynamic behavior [1] [35]. Models of the following components are generally needed in a composite model:

- Large industrial or commercial type induction motors

- Small appliance induction motors such as resident air conditioner compressors

- Discharging lights

- Heating and incandescent lighting load

- Thermostatically controlled loads

- Power electronic loads

- Transformer saturation effects

- Shunt capacitors

The composite load model also includes different representation for

- The percentage of each type of load components

- Parameter differences of similar load component types

- The parameters of the feeders such as impedance and admittance.

Each power operation management groups may have their own special composite load model for power system analysis. The composite model could also change with the different requirements. For example, the composite load model used by WECC in 2006 includes 20% induction motor load (dynamic), 80 % static load. Recently WECC has proposed a new composite load model that

includes transformers, shunt capacitors, feeder equivalent, three-phase induction

motors, and equivalent models for air conditioners [37].

3.3 Load model approaches

There are two commonly used methods to acquire the parameters of a load

model: measurement based and component based [1][38].

3.3.1 Measurement based

This method is considered a "top-down" approach. Measurements of

complex power, voltage, current, and frequency at the load bus can be used to

extrapolate parameters of the composite load model. These measurements may be

performed from staged tests, actual system transients, or continuous system

operation. The measurements can be utilized to determine the parameters of

Equations 3.1 - 3.8.

3.3.2 Component based

The component based approach was developed by Electric Power

Research Institute (EPRI) and is considered a "bottom-up" method. Composite

load model parameters are estimated by investigating and aggregating the detailed

characteristics of various types of system loads such as industrial, commercial,

residential, and agricultural.

EPRI also developed a program LOADSYN to automatically build up the

load model by aggregating the load performance. In [33] and [39], researchers

proposed and developed EPCL. EPCL is a programming language used in

General Electric's PSLF. It is able to automatically convert the different types of

load components in the power flow case to composite load models.

3.4   Induction motor

The induction machine is now widely used in appliances and industry. Because most of the grid's energy is consumed by the induction machine, it is important to understand its detailed static and dynamic characteristics.

Induction motors are normally represented as constant power load when in steady state operation. However, the constant power load model does not represent the motors response when a large disturbance occurs. Most stability study programs model induction motor dynamics with an equivalent circuit. This approach however is not able to correctly represent the induction motor for transient study.

3.4.1   Three-phase induction motor

3.4.1.1   Introduction

Three-phase induction motors are commonly used in industry. A typical three-phase induction motor contains two magnetically coupled windings: stator windings and rotor cage. When the stator winding is connected to three-phase power, a rotating magnetic field is created. The velocity of the rotating magnetic field is determined by the frequency of the power supply. Since frequency of the power system is well maintained, the rotating velocity of the magnetic field in the induction motor is almost constant and is called the synchronous velocity.

The rotor windings of three-phase induction motors are usually comprised of a cylindrical shaped conductor cage. The rotating magnetic field of the stator windings induces an alternating current in the rotor winding. Frequency of the induced current depends on the relative velocity between the synchronous field

and rotor rotational velocity. Torque is developed from the interaction of the two magnetic fields.

3.4.1.2   Equivalent circuit of three-phase induction motor

The simplified equivalent circuit of the three-phase induction motor is shown in Figure 3-1 [40]. In the figure, R_{sta} and X_{sta} are the stator resistance and reactance. R_{rot_s} and X_{rot_s} are the rotor resistance and reactance (referenced to the stator side). R_c and X_m are magnetizing resistance and reactance. The slip is calculated from:

$$s = \frac{W_{syn} - W_m}{W_{syn}} \tag{3.9}$$

where

w_{syn} - The synchronous angular speed of the magnetic field
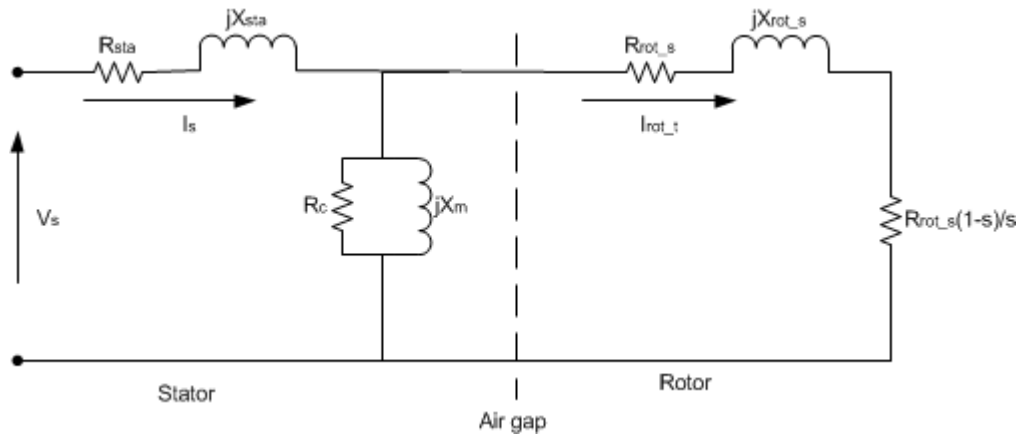
w_m - The angular speed of the motor

Figure 3-1 Simplified equivalent circuit of the three-phase induction motor

The motor synchronous speed is calculated as

$$W_{syn} = \frac{2\pi f}{p} \tag{3.10}$$

From Figure 3-1, the magnetizing impedance is calculated,

22

$$Z_{mag} = \frac{1}{\left[\left(\frac{1}{R_c}\right)+\left(\frac{1}{jX_m}\right)\right]} \tag{3.11}$$

The rotor impedance is calculated as

$$Z_{rot} = \frac{R_{rot\_s}}{s} + jX_{rot\_s} \tag{3.12}$$

The motor input current is then found by applying Ohm's Law.

$$I_s = V_s / \left[R_{sta} + jX_{sta} + \frac{Z_{mag}Z_{rot}}{(Z_{mag}+Z_{rot})}\right] \tag{3.13}$$

The motor input power is as follows:

$$S_s = P_s + jQ_s = V_s I_s{}^* \tag{3.14}$$

And the rotor current can be calculated with the following:

$$I_{rot} = I_s \frac{Z_{mag}}{(Z_{mag}+Z_{rot})} \tag{3.15}$$

The mechanical power supplied by the motor is the power dissipated in the slip load resistance minus the mechanical power loss.

$$P_{mech} = |I_{rot}|^2 * \frac{R_{rot}(1-s)}{s} - P_{Loss} \tag{3.16}$$

The load torque of the motor can then be determined.

$$T_m = p * \frac{P_{mech}}{W_m} \tag{3.17}$$

Here,

Z_{mag} - The magnetizing impedance for positive and negative slips

Z_{rot} - The rotor impedance

I_s - The motor input current

I_{rot} - The rotor current

S_s, P_s, Q_s - The motor input apparent, active, and reactive power

P_{mech} - The mechanical power supplied by the motor

T_m - The load torque of the motor

p - The number of magnetic pole pairs per phase

Simulations were conducted using the induction machine data provided on page 434 of [40]. The data is repeated in Table 3.1. Figure 3-2 presents the typical relationship between rotor speed, torque, input current magnitude, input active power, and input reactive power. The figure shows motor operation parameters corresponding to s = 3%. This is a constant torque situation. In some cases, the load torque may change with motor shaft speed.

Table 3.1 Equivalent circuit parameter values of three-phase induction motor

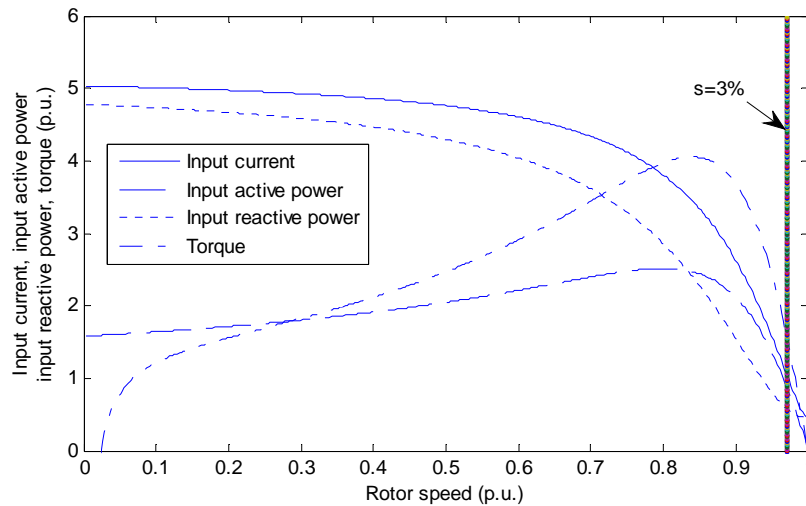|		
P_{motor} = 14.92 kW	V_{rms} = 254.034 V	V_{freq} = 60 Hz
R_{sta} = 0.44 Ω	X_{sta} = 1.25 Ω	$R_{rot\ s}$ = 0.4 Ω
$X_{rot\ s}$ = 1.25 Ω	R_c = 350 Ω	X_m = 27 Ω
P = 1	$P_{mech\ loss}$ = 262 W	P_{base} = 14.92 kW
V_{base} = 254.034 V	f_{base} = 60 Hz	I_{base} = P_{base}/V_{base}
Z_{basen} = $(V_{base})^2/P_{base}$	T_{base} = $P_{base}/(2\pi f_{base})$	

Figure 3-2 General characteristics of the three-phase induction motor

Parameters for the equivalent circuit can be determined using the

following measurements [40] [41]:

- No-load test

- Block-rotor test

- Stator resistance measurement

3.4.1.3   Mathematical model of three-phase induction motor

The three phase induction machine is usually expressed in dq0 coordinates according to the following power invariant abc -> dq0 transformation (Park's transformation). The zero sequence component is not included here because balanced operation is assumed [42].

$$\begin{bmatrix} V_{sd} \\ V_{sq} \end{bmatrix} = \sqrt{\frac{2}{3}} \begin{bmatrix} \cos\theta_{syn} & \cos(\theta_{syn} - \frac{2\pi}{3}) & \cos(\theta_{syn} - \frac{4\pi}{3}) \\ -\sin\theta_{syn} & -\sin(\theta_{syn} - \frac{2\pi}{3}) & -\sin(\theta_{syn} - \frac{4\pi}{3}) \end{bmatrix} \begin{bmatrix} V_a(t) \\ V_b(t) \\ V_c(t) \end{bmatrix} \quad (3.18)$$

In steady state, both components of the rotor voltage are zero.

$$\begin{bmatrix} V_{rd} \\ V_{rq} \end{bmatrix} = \begin{bmatrix} 0 \\ 0 \end{bmatrix} \quad (3.19)$$

Flux linkage can also be expressed in dq coordinates where the subscript s represents the stator and r corresponds to rotor quantities.

$$\lambda_{sd} = \frac{-1}{\omega_{syn}}\left(R_s i_{sq} - V_{sq}\right) \quad (3.20)$$

$$\lambda_{sq} = \frac{1}{\omega_{syn}}\left(R_s i_{sd} - V_{sd}\right) \quad (3.21)$$

$$\lambda_{rd} = \frac{-1}{s*\omega_{syn}} R_r i_{rq} \quad (3.22)$$

$$\lambda_{rq} = \frac{1}{s*\omega_{syn}} R_r i_{rd} \quad (3.23)$$

Stator and rotor currents are linearly related to flux linkages:

25

$$\begin{bmatrix} i_{sd} \\ i_{sq} \\ i_{rd} \\ i_{rq} \end{bmatrix} = \begin{bmatrix} L_s & 0 & L_m & 0 \\ 0 & L_s & 0 & L_m \\ L_m & 0 & L_r & 0 \\ 0 & L_m & 0 & L_r \end{bmatrix}^{-1} \begin{bmatrix} \lambda_{sd} \\ \lambda_{sq} \\ \lambda_{rd} \\ \lambda_{rq} \end{bmatrix} \qquad (3.24)$$

Torque is calculated as follows:

$$T_{em} = \frac{p}{2} L_m \left(i_{sq} i_{rd} - i_{sd} i_{rq} \right) \qquad (3.25)$$

Acceleration is related to torque and mechanical inertia (J_{eq}).

$$\frac{d}{dt} \omega_{mech} = \frac{T_{em} - T_L}{J_{eq}} \qquad (3.26)$$

Machine velocity is related to mechanical velocity through the number of poles.

$$\omega_m = \frac{p}{2} \omega_{mech} \qquad (3.27)$$

Slip is related to the difference between synchronous and machine velocity.

$$s = \frac{\omega_{syn} - \omega_m}{\omega_{syn}} \qquad (3.28)$$

Finally synchronous angle is related to synchronous velocity.

$$\frac{d}{dt} \theta_{syn} = \omega_{syn} \qquad (3.29)$$

where

$V_a(t)$ - Stator winding A phase voltage

$V_b(t)$ - Stator winding B phase voltage

$V_c(t)$ - Stator winding C phase voltage

θ_{syn} - Angle between d-axis and the stator a-axis

V_{sd} - Stator d-axis voltage transformed from $V_a(t)$, $V_b(t)$, $V_c(t)$

V_{sq} - Stator q-axis voltage transformed from $V_a(t)$, $V_b(t)$, $V_c(t)$

V_{rd} - Rotor d-axis voltage

V_{rq} - Rotor q-axis voltage

R_s - Average stator resistance per phase

R_r - Average rotor resistance per phase

ω_{syn} - Synchronous speed

λ_{sd} - Stator d-axis flux density

λ_{sq} - Stator q-axis flux density

λ_{rd} - Rotor d-axis flux density

λ_{rq} - Rotor q-axis flux density

i_{sd} - Stator d-axis current

i_{sq} - Stator q-axis current

i_{rd} - Rotor d-axis current

i_{rq} - Rotor q-axis current

L_s - Stator inductance per phase

L_r - Rotor inductance per phase

L_m - Mutual inductance

p - Number of poles

T_{em} - Instantaneous electromagnetic torque

T_L - Instantaneous load torque

ω_{mech} - Rotor speed in actual radians per second

J_{eq} - Motor inertia

ω_m - Rotor speed in electrical radians per second

This model is well known and validated [42][43]. It is often used in the
Simulink environment to represent dynamics of the three-phase cage rotor
induction machine.

3.4.2   Single-phase induction motor

3.4.2.1   Introduction

Single-phase induction motors are widely used in many household appliances. Generally, the single phase induction motor stator is composed of two separate windings: main (run) winding and auxiliary (start) winding that are physically displaced on the stator.

Single phase machines typically require extra circuitry to start. An auxiliary winding is needed to start single-phase induction motors because current flowing in the main winding cannot create a rotating field. Furthermore a phase displacement between the run and start winding currents is needed to create a rotating flux component. The start winding current is typically configured to lead relative to current in the run winding. After started, the run winding is able to keep the rotor spinning and the auxiliary winding is sometimes switched off when the motor reaches its operating speed. Different techniques of creating the needed phase displacement lead to different classifications of single-phase induction motors [44][45].

- Capacitor-start induction motor

    This type of motor is widely used and includes a capacitor connected in series with the auxiliary winding. The auxiliary winding is switched off at about 75% the nominal speed.

- Permanent-split capacitor motor

    This type of motor is similar to the capacitor-start machine except the auxiliary winding is connected in the circuit at all time. This machine

is characterized by good starting and running torque.

- Capacitor start/capacitor run motor

  A capacitor is connected in series with the auxiliary winding. At start up, the capacitance is higher by connecting two capacitors in parallel. After the motor reaches its nominal speed, one capacitor is switched off to improve running capability.

- Resistance split-phase induction motor

  The auxiliary winding of the motor is inductive like the main winding. However, the resistance to reactance ratio of the auxiliary winding is different from the resistance to reactance ratio of the main winding. Therefore main winding current and auxiliary winding current are not in phase and a rotating magnetic field is generated. The auxiliary winding is switched off when the motor reaches operating speed.

3.4.2.2   Equivalent circuit of single-phase induction motor

The simplified equivalent circuit of the single-phase induction motor is illustrated in Figure 3-3 [40]. As shown, R_{sta} and X_{sta} are the stator resistance and reactance. R_{rot_s} and X_{rot_s} are the rotor resistance and reactance transferred to the stator sides. R_c and X_m are magnetizing resistance and reactance. Finally positive and negative slip $(s_{pos}$ and $s_{neg})$ are defined as follows.

$$s_{pos} = \frac{W_{syn} - W_m}{W_{syn}} \qquad (3.30)$$

$$s_{neg} = \frac{W_{syn} + W_m}{W_{syn}} \qquad (3.31)$$

where

w_{syn} - The synchronous angular speed of the magnetic field

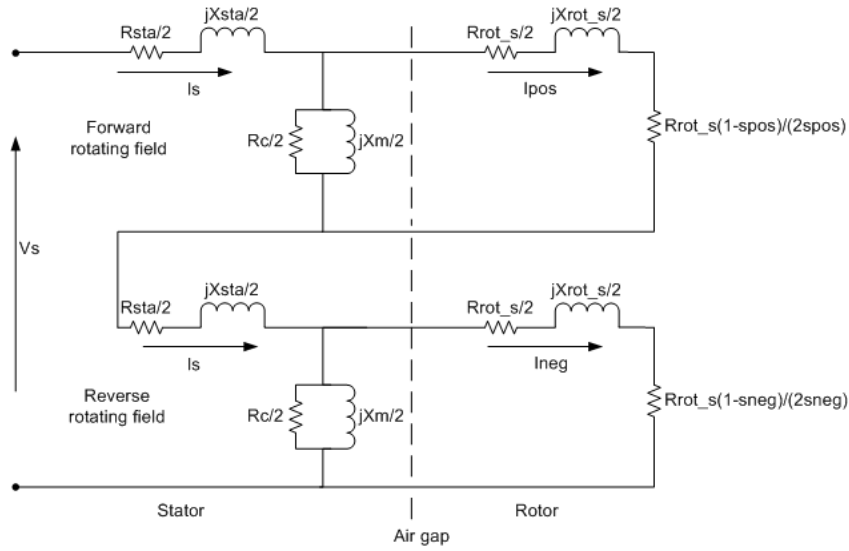w_m - The angular speed of the motor

Figure 3-3 Simplified equivalent circuit of the single-phase induction motor

The motor synchronous speed is calculated as

$$W_{syn} = \frac{2\pi f}{p} \qquad (3.32)$$

In reference to Figure 3-3, the magnetizing impedance is found and is the same for both positive and negative slip.

$$Z_{mag} = \frac{1}{\left[\left(\frac{1}{\frac{R_C}{2}}\right) + \left(\frac{1}{\frac{jX_m}{2}}\right)\right]} \qquad (3.33)$$

The rotor impedance for positive and negative slip is calculated as:

$$Z_{pos} = \frac{R_{rot\_s}}{2s_{pos}} + \frac{jX_{rot\_s}}{2} \qquad (3.34)$$

$$Z_{neg} = \frac{R_{rot\_s}}{2s_{neg}} + \frac{jX_{rot\_s}}{2} \qquad (3.35)$$

The motor input current is calculated by applying Ohm's Law.

$$I_s = V_s/[R_{sta} + jX_{sta} + \frac{Z_{mag}Z_{pos}}{(Z_{mag}+Z_{pos})} + \frac{Z_{mag}Z_{neg}}{(Z_{mag}+Z_{neg})}] \qquad (3.36)$$

30

The motor input complex power is:

$$S_s = P_s + jQ_s = V_s I_s{}^* \qquad (3.37)$$

Rotor currents for positive and negative slip are as follows:

$$I_{pos} = I_s \frac{Z_{mag}}{(Z_{mag} + Z_{pos})} \qquad (3.38)$$

$$I_{neg} = I_s \frac{Z_{mag}}{(Z_{mag} + Z_{neg})} \qquad (3.39)$$

The mechanical power supplied by the motor is the power dissipated in the two load slip resistances minus the mechanical power loss.

$$P_{mech} = |I_{pos}|^2 * \frac{R_{rot\_s}(1 - s_{pos})}{2s_{pos}} + |I_{neg}|^2 * \frac{R_{rot\_s}(1 - s_{neg})}{2s_{neg}} - P_{Loss} \qquad (3.40)$$

The load torque of the motor can then be determined.

$$T_m = p * \frac{P_{mech}}{W_m} \qquad (3.41)$$

Here,

Z_{mag} — The magnetizing impedance for positive and negative slip

Z_{pos} — The rotor impedance for positive slip

Z_{neg} — The rotor impedance for negative slip

I_s — The motor input current

I_{pos} — The rotor current for positive slip

I_{neg} — The rotor current for negative slip

S_s, P_s, Q_s — The motor input apparent, active, and reactive power

P_{mech} — The mechanical power supplied by the motor

T_m — The load torque of the motor

p — The number of magnetic pole pairs

31

Simulations were performed using models with parameters from page 469 of [40]. Figure 3-4 illustrates the typical relationship between rotor speed and torque, input RMS current, input active power, and input reactive power. In the figure Wr is the rotating speed of the motor in revolutions per minute (rpm).

Table 3.2 Equivalent circuit parameter values of single-phase induction motor

P_{motor} = 186.5 W	V_{rms} = 120V	V_{freq} = 60 Hz
R_{sta} = 2 Ω	X_{sta} = 2.5 Ω	$R_{rot\ s}$ = 4.1 Ω
$X_{rot\ s}$ = 2.2 Ω	R_c = 400 Ω	X_m = 51 Ω
P = 2	$P_{mech\ loss}$ = 50 W	P_{base} = 186.5 W
V_{base} = 120 V	f_{base} = 60 Hz	Z_{base}=$(V_{base})^2$/P_{base}
T_{base}=P_{base}/$(2\pi f_{base})$	I_{base}=P_{base}/V_{base}	

Figure 3-4 General characteristics of the single-phase induction motor
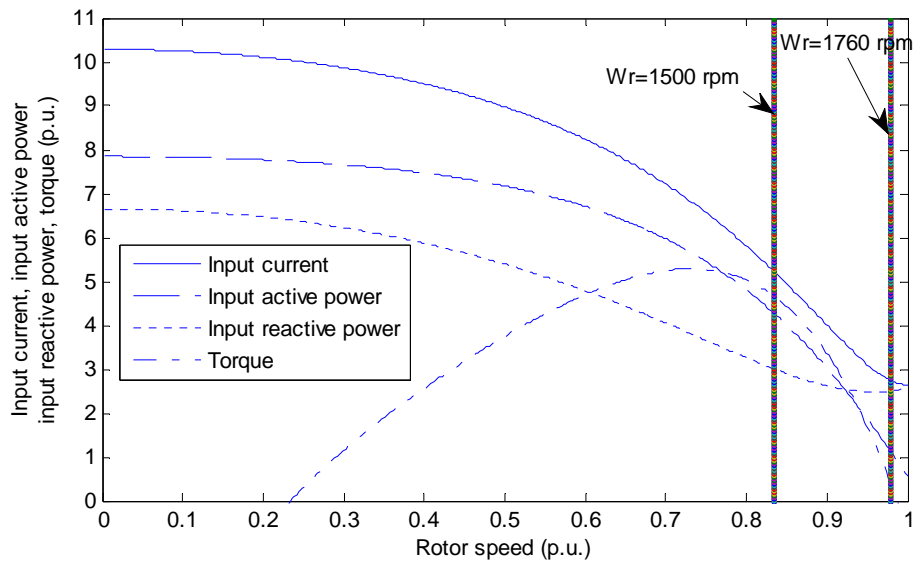
The parameters for equivalent circuit of the single-phase induction motor can be determined using a similar method as mentioned in Section 3.4.1.2.

3.4.2.3   Mathematical model of single-phase induction motor

A complete dynamic model for the single-phase motor models has been developed in the stationary reference frame [46]. By referring rotor parameters to

the stator side, the dynamics can be described as follows:

$$V_{as} = r_{as}i_{as} + \frac{d}{dt}\lambda_{as} \tag{3.42}$$

$$V_{bs} = r_{bs}i_{bs} + \frac{d}{dt}\lambda_{bs} \tag{3.43}$$

In steady state, both components of the rotor voltage are zero.

$$0 = r_r i_{ar} + \frac{d}{dt}\lambda_{ar} \tag{3.44}$$

$$0 = r_r i_{br} + \frac{d}{dt}\lambda_{br} \tag{3.45}$$

The rotor rotation speed depends on electrical torque, mechanic torque (load), and the motor inertia.

$$J\frac{d}{dt}\omega_r = T_{elec} - T_{mech} \tag{3.46}$$

The electrical torque is defined as follows:

$$T_{elec} = [i_{as} \quad i_{bs}]\begin{bmatrix} L_m & 0 \\ 0 & nL_m \end{bmatrix}\begin{bmatrix} -\sin(\theta) & -\cos(\theta) \\ -\cos(\theta) & \sin(\theta) \end{bmatrix}\begin{bmatrix} i_{ar} \\ i_{br} \end{bmatrix} \tag{3.47}$$

Parameters for the single phase induction machine are:

V_{as} - Stator main winding voltage

V_{bs} - Stator auxiliary winding voltage

i_{as} - Stator main winding current

i_{bs} - Stator auxiliary winding current

r_{as} - Stator main winding resistance

r_{bs} - Stator auxiliary winding resistance

λ_{as} - Stator main winding flux

λ_{bs} - Stator auxiliary winding flux

i_{ar} - Rotor main winding current

i_{br} - Rotor auxiliary winding current

r_r - Rotor winding resistance

λ_{ar} - Rotor main winding flux

λ_{br} - Rotor auxiliary winding flux

ω_r - Rotor speed

J - Motor inertia

T_{elec} - Electrical torque

T_{mech} - Mechanical load torque

N - The ratio of stator auxiliary winding turns to stator main winding turns

L_m - Stator magnetizing inductance

θ - Rotor angle

A transformation is applied such that the fundamental frequency of all parameters is equal to the source frequency.

$$\begin{bmatrix} ds \\ qs \end{bmatrix} = \begin{bmatrix} 1 & 0 \\ 0 & 1 \end{bmatrix} \begin{bmatrix} as \\ bs \end{bmatrix} \tag{3.48}$$

$$\begin{bmatrix} dr \\ qr \end{bmatrix} = \begin{bmatrix} \cos(\theta) & -\sin(\theta) \\ -\sin(\theta) & -\cos(\theta) \end{bmatrix} \begin{bmatrix} ar \\ br \end{bmatrix} \tag{3.49}$$

The winding dynamic equations become:

$$V_{ds} = r_{ds} i_{ds} + \frac{d}{dt} \lambda_{ds} \tag{3.50}$$

$$V_{qs} = r_{qs} i_{qs} + \frac{d}{dt} \lambda_{qs} \tag{3.51}$$

$$0 = r_r i_{dr} - \omega_r \lambda_{qr} + \frac{d}{dt} \lambda_{dr} \tag{3.52}$$

$$0 = r_r i_{qr} + \omega_r \lambda_{dr} + \frac{d}{dt} \lambda_{qr} \tag{3.53}$$

$$J \frac{d}{dt} \omega_r = T_{elec} - T_{mech} \tag{3.54}$$

34

Where $r_{ds} = r_{as}$ and $r_{qs} = r_{bs}$.

The electric torque can then be calculated as:

$$T_{elec}$$

$$= [i_{ds} \quad i_{qs}] \begin{bmatrix} L_m & 0 \\ 0 & nL_m \end{bmatrix} \begin{bmatrix} -\sin(\theta) & -\cos(\theta) \\ -\cos(\theta) & \sin(\theta) \end{bmatrix} \begin{bmatrix} \cos(\theta) & -\sin(\theta) \\ -\sin(\theta) & -\cos(\theta) \end{bmatrix} \begin{bmatrix} i_{dr} \\ i_{qr} \end{bmatrix}$$

$$= L_m i_{ds} i_{qr} - nL_m i_{qs} i_{dr} \tag{3.55}$$

This model is capable of providing accurate behavior of the single-phase motor in transient study.

3.4.3 Particular characteristics of induction motor load

When the voltage applied to the motor is reduced as a result of transmission or distribution faults, the electrical torque generated by the motor will also be reduced. This in turn slows the motor. The rate of deceleration is dependent on the motor inertia and load torque. If the applied voltage is too low or if the duration is too long, the motor will stop rotating (stall). Stalled motors draw an abnormally high current from the grid.

To reduce adverse effects on the grid, two types of protection are typically employed. Under Voltage Protection (UVP) is a circuit with a contactor to trip the motor offline when the applied voltage is below a certain level. Thermal Over Load (TOL) protection disconnects the motor if it becomes too hot as a result of an extended stall condition.

CHAPTER 4

MODELING AND SIMULATION OF RESIDENTIAL AIR CONDITIONERS

This chapter describes RAC characteristics, their influence on system

operation, and requirements for modeling RACs. The latest modeling methods for

RACs are presented. Voltage sag events are also simulated and compared for both

single and three phase motor models.

4.1   Introduction of residential air conditioner (RAC) motors

The most common type of motor used in RACs is compressor-driving,

capacitor-start or capacitor-run single-phase induction machine. A few compressor

motors include a starting kit that enhances starting torque. The RAC compressor

is normally either reciprocating or scroll type. The reciprocating compressor is

used by most of the RACs in the United States, but the scroll type is becoming

more popular.

References [33][34][49] and [50] present test results of RACs with a

variety of compressor technology, tonnage, efficiency, and refrigerant. Typical

behaviors of the RACs are observed:

- Under steady-state condition, the power consumed by the RAC is used

  80-87% by the compressor motor, 10–12% by indoor fan, and 3–5%

  by outdoor fan.

- The high efficiency, low inertia single-phase motors used by RACs are

  prone to stall quickly.

- Under stall condition, the RACs draw very high current. Much active

  and reactive power is consumed when stalled.

- The RAC is likely to stall when the applied voltage is between 50% and 73% of its nominal voltage and voltage sag duration is equal or more than 3 cycles. The stalling threshold voltage depends on the outdoor temperature.

- The RAC is normally equipped with the TOL protection. According to lab experiments on different type of RACs, the time duration was found to be about 5 to 20 seconds in [33]; about 1 to 20 seconds in [34]; about 6 to 18.5 seconds reported by EPRI, about 2 to 20 seconds by SCE in [49]; and about 2 to 46 seconds in [50].

- The RAC is also equipped with UVL. The dropout voltage was discovered to be about 43% to 56% in [33]; about 35% to 55% in [34] ; an average of 52% found by EPRI; 42% by SCE in [49]; and about 35% to 45% in [50].

- Under stalled conditions, if the compressor motor used by RAC is a scroll unit, the motor may restart automatically if the applied voltage recovers quickly enough (approximately above 70%). If the compressor motor used by RAC is a reciprocating unit, the motor will not restart by itself.

4.2   Why modeling RAC motors are important

The investigation of FIDVR events in some cases shows that the stalling of RACs after a system fault is the primary cause [29]-[34]. Results from testing of 28 air conditioner units [34] indicate more detail as to why this occurs. After a voltage sag, the low-inertia air conditioners stall quickly and the increased stall

power further deteriorates the system voltage. If the voltage sag is above the UVL threshold, system voltage will recover only after the TOL protection has disconnected the units.

Conventionally, the single-phase air conditioner motors are represented by three-phase induction motors. After studying a number of FIDVR events, SCE and WECC concluded that three-phase induction motor models do not accurately represent the characteristics of air conditioner loads in stability simulations [50]. Thus the creation of a precise aggregate model of the single-phase induction machine becomes an urgent issue.

4.3   Model requirements

The basic requirement for the RAC model is to accurately represent the steady and dynamic behavior of the RAC unit. Reference [46] and [50] introduced RAC systematic model requirements specified by WECC LMTF as follows:

- Model should be computationally stable with ¼ cycle simulation time step as commonly used in transient stability studies.

- In steady state the RAC active and reactive power should be represented precisely for slow voltage variations.

- When oscillation occurs, the RAC active and reactive power should be represented reasonably for frequency oscillations up to 1.0 Hz.

- When the motor stalls, the current, active power, and reactive power consumed by the RACs should be represented well.

- When voltage sag occurs, the model should distinguish and accurately represent the complex power during stall and re-acceleration.

- The model should be able to accurately represent TOL tripping as a function of the current and time.

- Represent reasonably the control operation of the motor.

4.4   Modeling RAC compressors

4.4.1   Classification of RAC models

Many techniques for modeling the RAC motor have been presented. Generally, models can be categorized as equipment or grid level type [46] [50].

- Equipment-level models:

   The equipment-level models represent only one unit and describe RAC behavior in detail with high accuracy. The models introduced in Section 3.4.1, Section 3.4.2, and the phasor model to be discussed are all considered equipment-level models. However it is impractical to represent each RAC with an equipment-level model because of excessive simulation time.

- Grid-level models:

   Grid-level models represent many RAC motors as an aggregate. Usually precision is lacking in this type of model. The grid-level model is commonly used in power system simulators.

4.4.2   Phasor model

RACs usually contain a single phase induction motor driving a compressor load. Since the magnetic field produced by the windings is normally not symmetric, simplifying operations like Park's dq0 transformation cannot be applied.

The mathematical model of Section 3.4.2.3 was used a basis in the development of a phasor model [46]. This model was created with the technique of dynamic phasor representation. This model is an approximation but is still correctly represents RAC operation in steady-state and transient. The simplification however neglects higher-order harmonics and fast transients. Also the phasor model takes into account saturation effects and captures the detailed electrical behavior of the motor. The equations are as follows [46]:

$$|V_s| = \left(r_{ds} + j\frac{w_s}{w_b}X_{ds}'\right)\left(I_{ds}{}^R + jI_{ds}{}^I\right) + j\left(\frac{w_s}{w_b}\right)\left(\frac{X_m}{X_b}\right)\left(\Psi_{dr}{}^R + j\Psi_{dr}{}^I\right) \tag{4.1}$$

$$|V_s| = \left(r_{qs} + j\frac{w_s}{w_b}X_{qs}' + j\frac{w_s}{w_b}X_c\right)\left(I_{qs}{}^R + jI_{qs}{}^I\right) + j\left(\frac{w_s}{w_b}\right)\left(\frac{nX_m}{X_r}\right)\left(\Psi_{qr}{}^R + j\Psi_{qr}{}^I\right)$$
$$\tag{4.2}$$

$$\begin{bmatrix} \left(\Psi_f{}^R + j\Psi_f{}^I\right) \\ \left(\Psi_b{}^R + j\Psi_b{}^I\right) \end{bmatrix} = \frac{1}{2}\begin{bmatrix} 1 & -j \\ 1 & j \end{bmatrix}\begin{bmatrix} \left(\Psi_{dr}{}^R + j\Psi_{dr}{}^I\right) \\ \left(\Psi_{qr}{}^R + j\Psi_{qr}{}^I\right) \end{bmatrix} \tag{4.3}$$

$$\begin{bmatrix} \left(\Psi_{dr}{}^R + j\Psi_{dr}{}^I\right) \\ \left(\Psi_{qr}{}^R + j\Psi_{qr}{}^I\right) \end{bmatrix} = \begin{bmatrix} 1 & 1 \\ j & -j \end{bmatrix}\begin{bmatrix} \left(\Psi_f{}^R + j\Psi_f{}^I\right) \\ \left(\Psi_b{}^R + j\Psi_b{}^I\right) \end{bmatrix} \tag{4.4}$$

$$\begin{bmatrix} \left(I_f{}^R + jI_f{}^I\right) \\ \left(I_b{}^R + jI_b{}^I\right) \end{bmatrix} = \frac{1}{2}\begin{bmatrix} 1 & -jn \\ 1 & jn \end{bmatrix}\begin{bmatrix} \left(I_{ds}{}^R + jI_{ds}{}^I\right) \\ \left(I_{qs}{}^R + jI_{qs}{}^I\right) \end{bmatrix} \tag{4.5}$$

$$\begin{bmatrix} \left(I_{ds}{}^R + jI_{ds}{}^I\right) \\ \left(I_{qs}{}^R + jI_{qs}{}^I\right) \end{bmatrix} = \frac{1}{2}\begin{bmatrix} 1 & 1 \\ j/n & -j/n \end{bmatrix}\begin{bmatrix} \left(I_f{}^R + jI_f{}^I\right) \\ \left(I_b{}^R + jI_b{}^I\right) \end{bmatrix} \tag{4.6}$$

$$T_o'\frac{d}{dt}\left(\Psi_f{}^R + j\Psi_f{}^I\right) = X_m\left(I_f{}^R + jI_f{}^I\right) -$$
$$\left(sat(\Psi_f, \Psi_b) + j(w_s - w_r)T_o'\right)\left(\Psi_f{}^R + j\Psi_f{}^I\right) \tag{4.7}$$

$$\left(\Psi_b{}^R + j\Psi_b{}^I\right) = \frac{X_m\left(I_b{}^R + jI_b{}^I\right)}{\left(sat(\Psi_f,\Psi_b) + j(w_s + w_r)T_o'\right)} \tag{4.8}$$

$$\frac{2H}{w_b}\frac{dw_r}{dt} = \frac{X_m}{X_r}2\left(I_f{}^I\Psi_f{}^R - I_f{}^R\Psi_f{}^I - I_b{}^I\Psi_b{}^R + I_b{}^R\Psi_b{}^I\right) - T_{mech} \tag{4.9}$$

$$I_s = \left[\left(I_{ds}{}^R + jI_{ds}{}^I\right) + \left(I_{qs}{}^R + jI_{qs}{}^I\right)\right]e^{j\varphi} \qquad (4.10)$$

$$sat\left(\Psi_f, \Psi_b\right) = \begin{cases} 1 & for\ \Psi \leq b_{sat} \\ 1 + A_{sat}(\Psi - b_{sat})^2 & for\ \Psi > b_{sat} \end{cases} \qquad (4.11)$$

$$\Psi = \sqrt{\left(\Psi_f{}^R\right)^2 + \left(\Psi_f{}^I\right)^2 + \left(\Psi_b{}^R\right)^2 + \left(\Psi_b{}^I\right)^2} \qquad (4.12)$$

where

V_s - Applied voltage Phasor

ω_s - Applied voltage frequency

ω_b - Frequency base

φ - Applied voltage phase angle

H - Motor inertia

N - Ratio of stator auxiliary winding turns to stator main winding turns

T_{mech} - Mechanical load torque

r_{ds} - d-axis stator resistance

r_{qs} - q-axis rotor resistance

X_{ds}' - d-axis stator transient reactance

X_{qs}' - q-axis stator transient reactance

X_m - Magnetizing reactance

X_r - Rotor reactance

X_c - Capacitive reactance

A_{sat} - Saturation constant

b_{sat} - Saturation constant

ω_r - Motor speed

$I_{ds}{}^R$ - Real part of d-axis stator current

$I_{ds}{}^{I}$ - Imaginary part of d-axis stator current

$I_{qs}{}^{R}$ - Real part of q-axis stator current

$I_{qs}{}^{I}$ - Imaginary part of q-axis stator current

$\Psi_{ds}{}^{R}$ - Real part of d-axis rotor flux voltage

$\Psi_{ds}{}^{I}$ - Imaginary part of d-axis rotor flux voltage

$\Psi_{qs}{}^{R}$ - Real part of q-axis rotor flux voltage

$\Psi_{qs}{}^{I}$ - Imaginary part of q-axis rotor flux voltage

Ψ_{f}^{R} - Real part of forward rotating flux voltage

Ψ_{f}^{I} - Imaginary part forward rotating flux voltage

$\Psi_{b}{}^{R}$ - Real part of backward rotating flux voltage

$\Psi_{b}{}^{I}$ - Imaginary part of backward rotating flux voltage

I_{f}^{R} - Real part of forward current

I_{f}^{I} - Imaginary part forward current

I_{b}^{R} - Real part of backward current

I_{b}^{I} - Imaginary part of backward current

I_{s} - Stator current

$T_{o}{}'$ - Represent $\dfrac{x_r}{w_b R_r}$

Satt(Ψ_f, Ψ_b)   - Saturation function

       The example simulations in reference [46] show that the phasor model is able to demonstrate machine dynamics and stall behavior. It has also been shown that this model can represent the air conditioner load during both steady-state and transient.

       The phasor model also satisfies the WECC LMTF model requirements

described in Section 4.3. The phasor model is being considered by WECC as a primary approach for modeling RACs.

4.4.3   Grid-level models

The most common methods for grid-level modeling are performance and hybrid.

4.4.3.1   Performance based method

The performance based method is a reasonable way to approximate the aggregate behavior of motors. The active and reactive power needed by the motors are measured and recorded in many different voltage and frequency conditions. These values are able to represent the motor behavior during the slow transients (up to 0.5 Hz). When the power supply is above the stall voltage level, the motor can be considered as a "running" model. When the supply voltage falls below the stall voltage threshold, the "running" model is replaced with a "stalled" model [50]. The switching time between "running" and "stalled" models (a few cycles) is neglected as it is assumed that not much information is lost during the transition.

4.4.3.2   Hybrid model

A hybrid model was proposed in [33],[38] [51], and [52] to represent the RACs for the simulation. This model was derived from observed behavior reported in [49]. The hybrid model of the RACs is normally composed of two parallel connected components:

- A standard three-phase induction motor model that represents reasonable steady-state and dynamic behavior of aggregated RACs in normal operation.

- A constant shunt impedance load that represents stalled behavior.

In normal operation the RACs are represented with the standard three-phase induction motor model. After stall, the constant shunt impedance is switched on instead.

The shunt impedance load is usually determined by the normal operation load, the rated locked-rotor current, and estimated power factor under stall conditions [52]. The shunt impedance is configured to draw, at reduced voltage, about two to three times of the rated current. The reactance and resistance of the shunt are typically both about 20% of the motor reactance and resistance at rated voltage [33].

In [33] the hybrid model was validated using the data from an observed delayed voltage recovery event in 2003. The hybrid model proposed in [52] assumes the shunt impedance power factor is 0.45. This is common in present energy-efficient RAC motors under stall conditions. Reference [51] utilized the hybrid model to investigate mitigating adverse effects of FIDVR events.

The grid level model is very practical to represent the motor load at steady state and stall for simulation of the large power system. However the transient response of the motor load is missing and this may be very important to voltage transient stability.

4.5   Motor modeling and parameters

A single phase phasor model and a three phase motor model were simulated to find the best representation of RAC behavior in presence of voltage sags.

4.5.1   Single-phase induction motor parameters and simulation

The phasor model previously discussed is appropriate to represent air conditioner load in steady-state and transient. The phasor model of a typical air conditioner from [46] was selected for simulation. Parameters of this model are listed below.

Table 4.1 Parameters for phasor model

P_{base} = 3500 W	V_{base} = 240 V	I_{base} = 14.5833 A	Z_{base} = 16.4571 Ω
ω_s = 377 rad/sec	ω_b = 377 rad/sec	r_{ds} = 0.0365 p.u.	X_{ds}' = 0.1033 p.u.
r_{qs} = 0.0729 p.u.	X_{qs}' = 0.1489 p.u.	X_c = -2.779 p.u.	X_m = 2.28 p.u.
r_r = 0.0486 p.u.	X_r = 2.33 p.u.	H = 0.04 Ws/VA	n = 1.22
A_{sat} = 5.6	b_{sat} = 0.7212	T_o' = 0.1212 p.u.	T_{mech}= 0.85+ $(\omega_r/\omega_b)^4$ p.u.

In this model, T_{mech} is a function of rotor speed and H falls within the 0.03 sec to 0.05 sec range suggested by laboratory tests [34][49].

The phasor model was simulated in Simulink under momentary voltage sag conditions without TOL or UVL protection logic. Figure 4-1 illustrates results of the RAC phasor model under two voltage sag cases. Figure 4-1 (a) shows the input RMS voltage for .4 p.u. and .65 p.u. voltage sag cases. Both sags occur at 1.334 s with five cycle duration. Figure 4-1 (b), (c), and (d) show the active power, reactive power, and the motor's rotation speed.
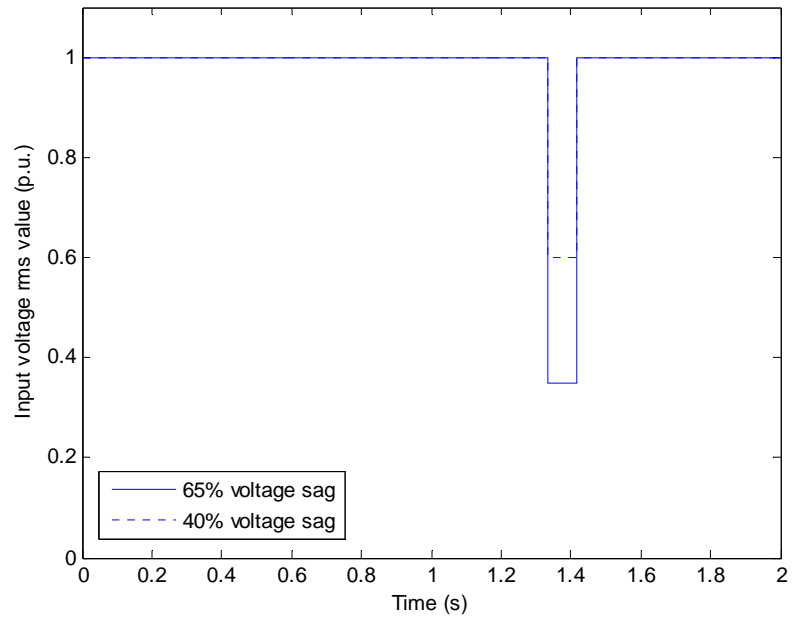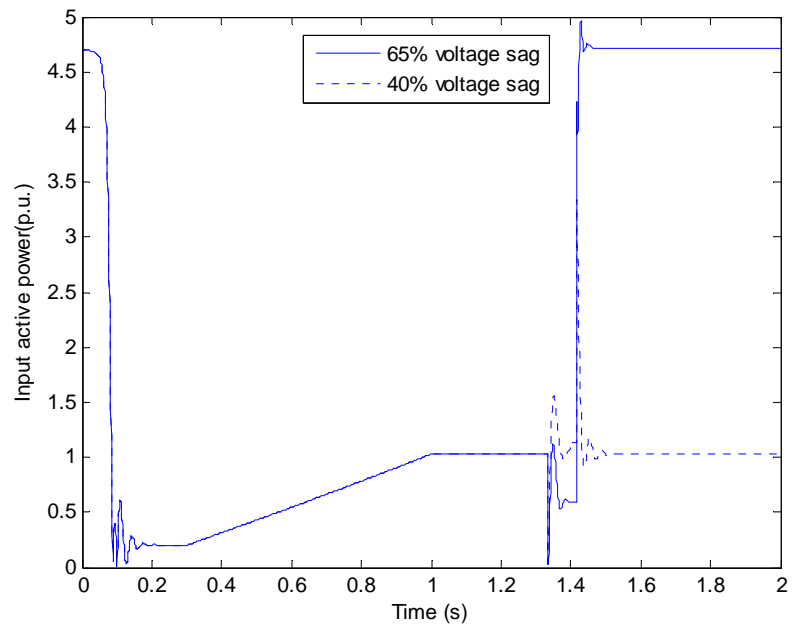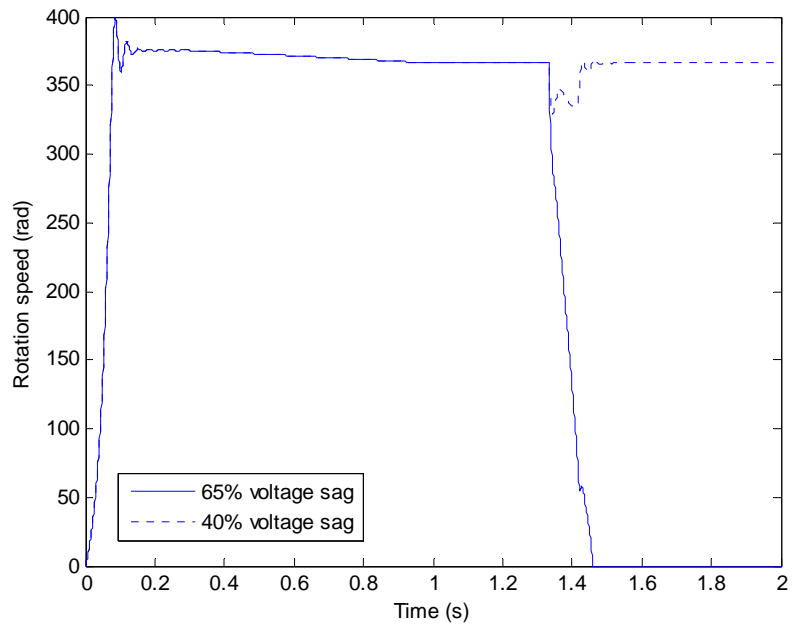
45

(a) The RMS value of the input voltage (p.u.)

(b) The input active power (p.u.)
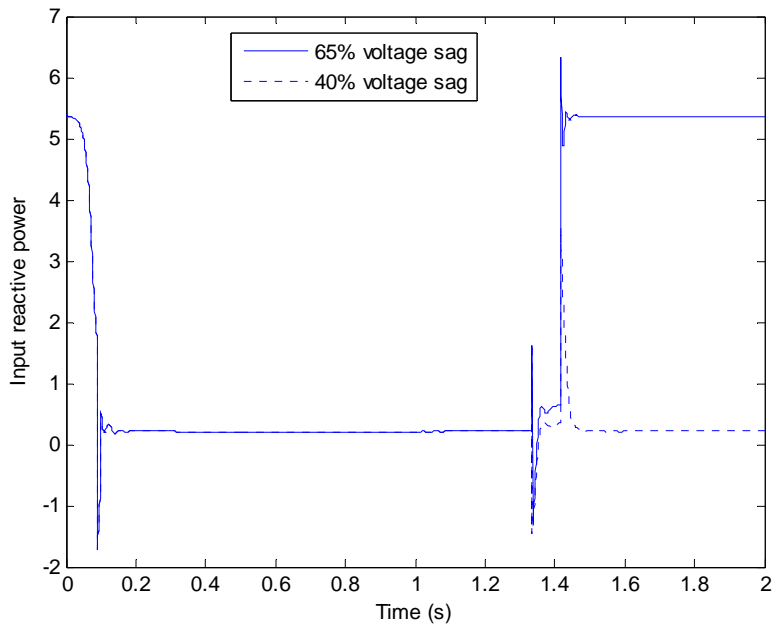
(c) The input reactive power (p.u.)

(d) The rotation speed of the rotor (rad/s)

Figure 4-1 Simulation result of phasor model

The figure shows that the starting power is around five times steady state. In the case of 40% voltage sag, the RMS current increased more than two times normal operation. The rotation speed also recovered in the 40% voltage sag case. In the 65% case, the motor stalled resulting in a significant increase of active and reactive power consumption.

4.5.2   Three-phase induction motor parameters and simulation

A three-phase motor model was also tested in simulation. The model has no startup control and its load torque (T_{mech}) was set constant. Table 4.2 lists the parameters used in simulation.

Table 4.2 Parameter values of three-phase induction motor

S_{base} = 100 MVA	V_{base} = 230 kV	f_{base} = 60 Hz	T_{mech} = 0.5
R_s = 0.01 p.u.	X_s = 0.15 p.u.	R_r = 0.05 p.u.	X_r = 0.15 p.u.
X_m = 5 p.u.	H = 3 kWs/kVA		

Here R_s and X_s are stator resistance and reactance respectively. The cage rotor resistance and reactance are R_r and X_r respectively. X_m is the magnetization reactance, H is the inertia constant, and T_{mech} is the mechanic load torque.

Figure 4-2 illustrates simulation results of a three-phase motor model under voltage sags of one second, and five cycle duration. The first voltage sag is to 0.1 p.u., and the second to 0.5 p.u. Figure 4-1 (a) shows the input RMS voltage. Figure 4-1 (b), (c), and (d) present the consumed active power, reactive power, and rotor rotation speed respectively. Larger voltage sags were used here to show how resilient the three phase motor is in the presence of such disturbances.
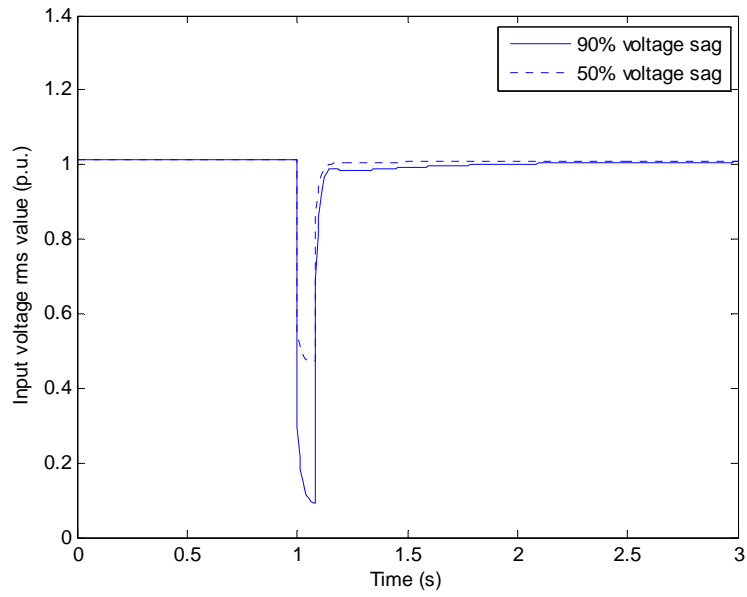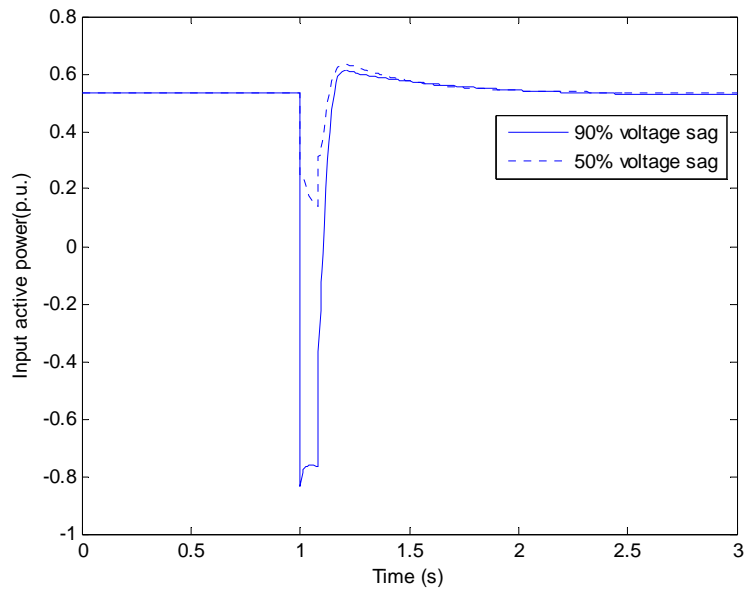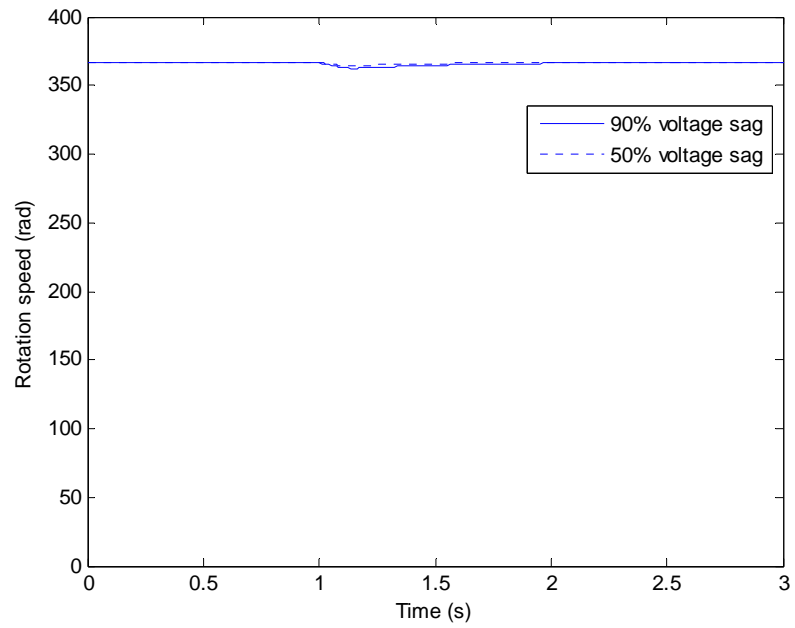
48

(a) The RMS value of the input voltage (p.u.)

(b) The input active power (p.u.)
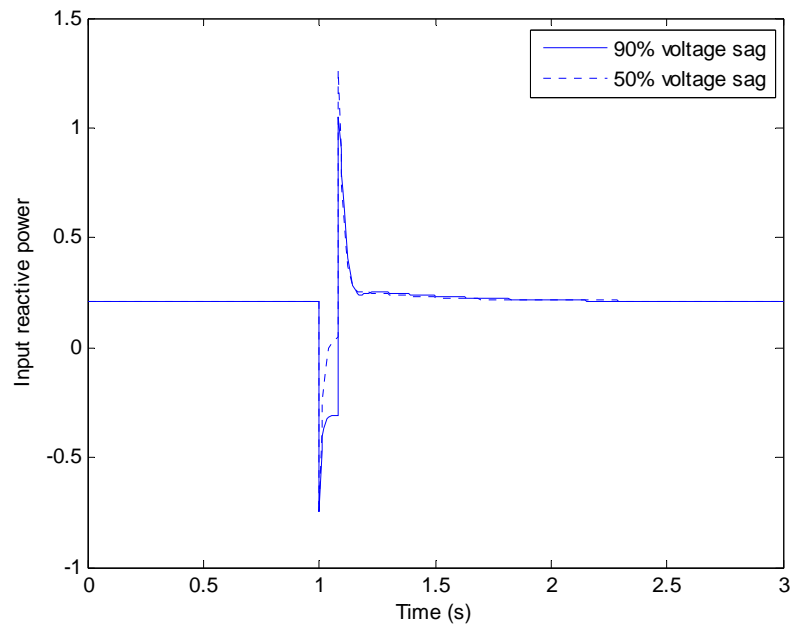
(c) The input reactive power (p.u.)

(d) The rotation speed of the rotor (rad/s)

Figure 4-2 Simulation result of three-phase motor model

Simulation results show the rotation speed of this three-phase motor is almost constant even with 90 % voltage sag. Also the active power and reactive power consumed by the three-phase motor increased during the fault.

CHAPTER 5

PROPOSED METHOD

5.1   Overview

The objective of this work is to compare detailed single phase motor loads

with the typical three phase motor aggregate approximation. The context of the

study is voltage stability and in particular fault induced voltage recovery. A

technique to interface a typical positive sequence power flow simulation with

detailed single phase motor models is presented.

5.2   Proposed method for simulation of single-phase induction motor

The proposed solution utilizes the detailed single-phase equipment level

models of distribution networks to replace the grid level aggregate equivalent load

model in a typical positive sequence power system simulation tool. The proposed

method involves an interface between the transmission network power flow

simulation and a detailed distribution model. The detailed distribution system for

this study was configured with constant impedance load and unit level

single-phase induction motor load. The distribution networks were connected to

the bus nodes in the transmission network.

As shown in Figure 5-1, the simulation of the power system operation is

realized by dividing the total simulation duration into many short time periods.
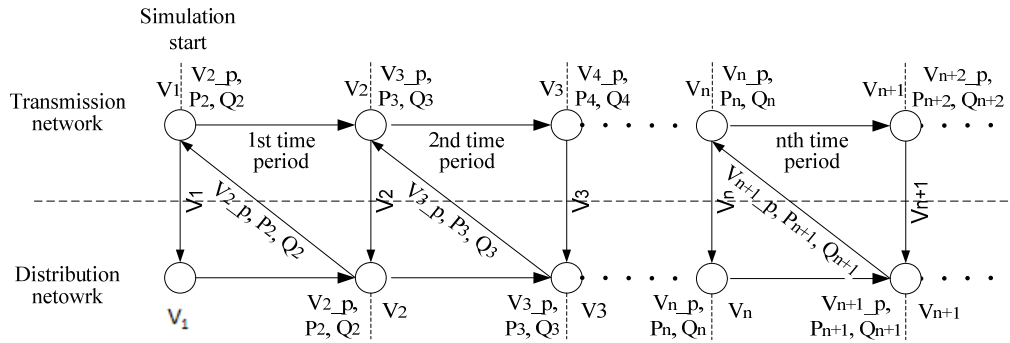
Figure 5-1 The simulation procedure of the power system

Data from the transmission network and the data from the distribution network are exchanged in each time period. This data communication ensures continuity of power system dynamic study. For each time period a procedure is repeated. In the first time period,

- Perform the power flow analysis of the transmission network and record the bus voltage (V_1) of the selected bus

- Provide the magnitude and angle of V_1 to the distribution system as the supply voltage

- Run the time-domain simulation of the distribution network in the first time period and record the positive sequence of the supply voltage (V_{2_p}), active load (P_2), and reactive load (Q_2) at the end of the time period

- In transmission network, replace V_1 with the V_{2_p}, and update the bus load with P_2 and Q_2

- The transmission network is then ready for the time-domain simulation in the first time period

53

This procedure is continuously repeated in each time step until the simulation end. This method gives a precise representation of the bus load and voltage change in the transmission network in transient and steady state. Simulation results of various load composition of the distribution network will be compared and analyzed.

5.3   Simulation software

The proposed method was applied to power system simulation using two simulators: PSAT and MATLAB SIMULINK. The transmission network was simulated using the PSAT and the distribution network was built in MATLAB SIMULINK. These two simulators were selected to perform the proposed method because of simple data exchange between the two.

CHAPTER 6

CASE STUDIES

6.1   Overview

In this work, the effects of single-phase motor load on voltage stability are investigated. Differences between typical equivalent three phase motor aggregate approximations and detailed single phase motor loads are studied. A power system with different percentage of equivalent three phase and single phase motor loads was designed and built in simulation.

The three phase motor model introduced in Section 4.5.2 was utilized to represent an aggregate approximation of single phase motors. For capturing the accurate transient response of the motor load, the equipment-level phasor model introduced in Section **Error! Reference source not found.** was used to represent the single-phase motor load.

Figure 6-1shows the distribution network built in simulation for single-phase loads. The distribution system is simplified in this research as it does not take into account the feeders, distribution capacitors, protection, etc.
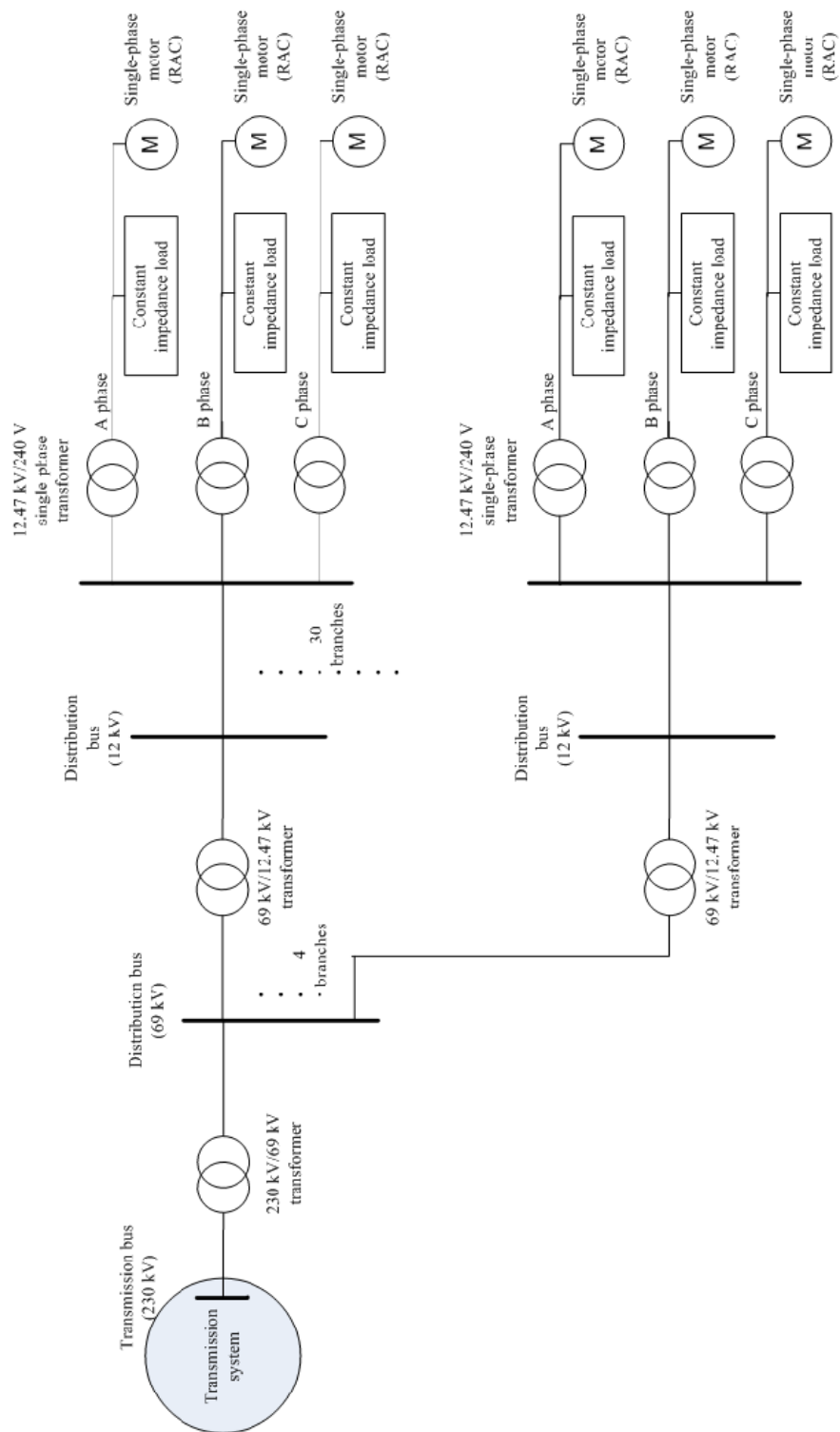
Figure 6-1 Distribution system with single-phase motor load

The simulated distribution system is a star network and includes:

- One 230 kV / 69 kV three-phase transformers

- Four 69 kV / 12.47 kV three-phase transformers

- Three hundred and sixty 12.47 kV / 240 V single-phase transformers

- Load components

6.2   The transmission system

The objective of the proposed method is to study the influence of motor load on the actual power system. Accordingly the WECC 3-machine, 9-bus system with turbine governor and AVR, was built in PSAT for this case study. In this test system, the power base is 100 MVA and frequency is 60 Hz. The system includes:

- 9 lines

- 3 PQ buses (Bus 5, 6, and 8)

- 2 PV buses (Bus 2 and 3)

- 3 machines with governors and AVR (Bus 1, 2, and 3)

- The swing bus is Bus 1

6.3   Simulation cases

A normally-cleared short duration fault was selected as the contingency for analyzing the motor effects on power system stability. The fault is defined as follows:

- At t=1 s, a three-phase grounding fault occurs on bus 7

- The circuit breaker installed between bus 4 and bus 7 clears the fault at 1.083 second (after 5 cycles)

Bus 6 of the transmission network was selected as the load bus. The load was set as 0.762 + j0.304 p.u. to represent a mixed composition. The power factor of this load is 0.93.
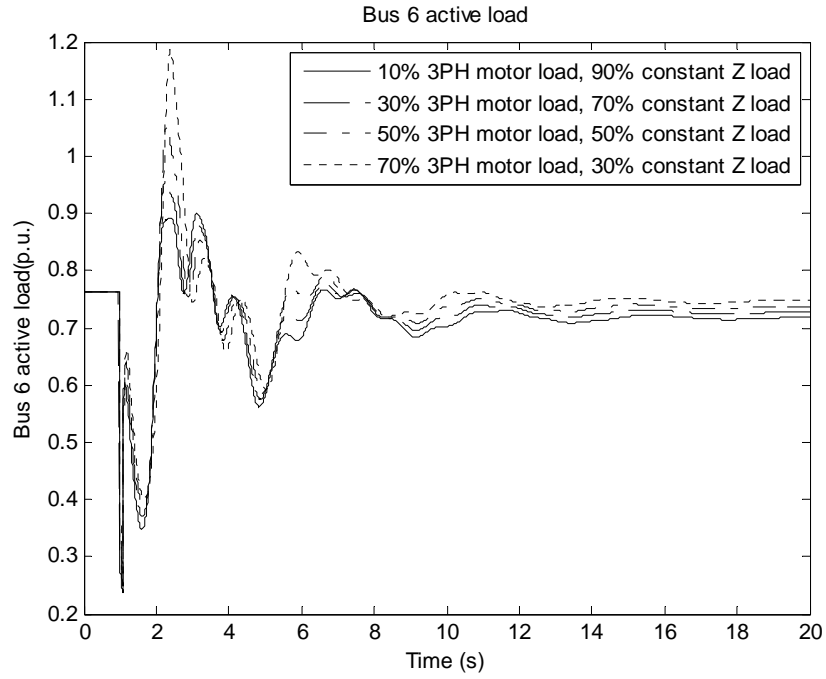
6.3.1   Three-phase motor load

The tests in this section are to analyze the influence of three-phase motor load on the power system. It is assumed that all the single phase motor loads in the distribution system are represented as an equivalent three-phase motor load. Four different load test cases were configured for bus 6.

Table 6.1 Three-phase motor loads on bus 6

Case number	Constant Z load (%)	Motor load (%)	Motor type	Motor P (p.u.)	Motor Q (p.u.)
1	90	10	Three-phase	0.0762	0.0304
2	70	30	Three-phase	0.2285	0.0911
3	50	50	Three-phase	0.3809	0.1518
4	30	70	Three-phase	0.5332	0.2125

Simulation results of the four load cases are shown in Figure 6-2. After the fault is cleared, the active loads oscillate and slowly returned to a stable state. The reactive load power shows spikes when the fault occurs and when it is cleared. By the end of this 20 seconds simulation, the loads in the four test cases are slightly different because the amount of actual motor load is affected by power flow calculation in the post-fault transmission network.

(a) Bus 6 load active power
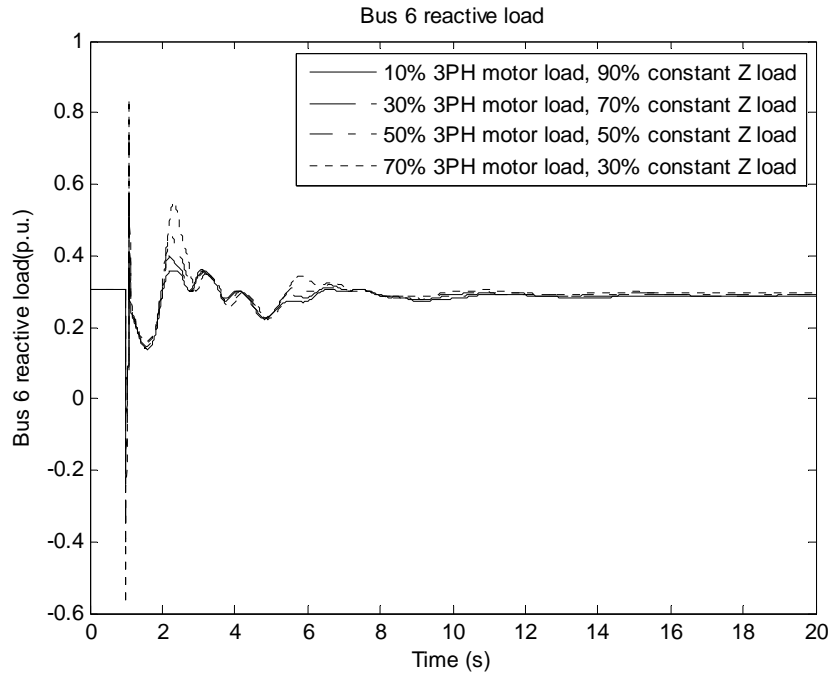
(b) Bus 6 load reactive power

Figure 6-2 Bus 6 load power for three-phase motor load

59

The voltage magnitude and angles at bus 6 corresponding to different

motor load percentage are shown in Figure 6-3 and Figure 6-4.

Figure 6-3 shows that the voltage in all cases initially recovered to about

90% and then reduced to around 0.65 p.u.. Some ringing can be seen as the

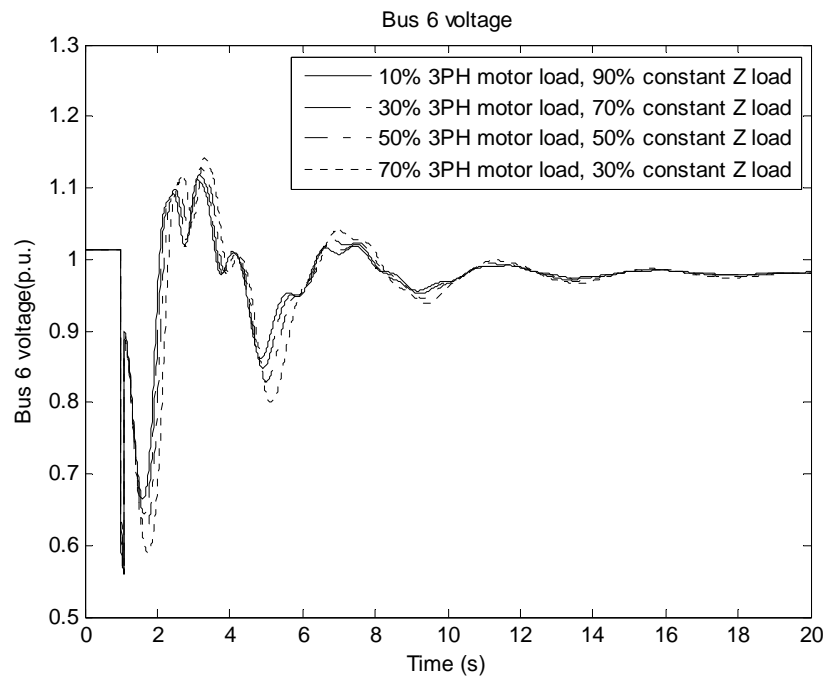voltage returned to a stable value of 0.98 p.u..

Figure 6-3 Bus 6 voltage magnitude for three-phase motor load

The bus angles presented in Figure 6-4 shows the angle difference

between bus 6 and the swing bus. After the fault, the angle difference spiked then

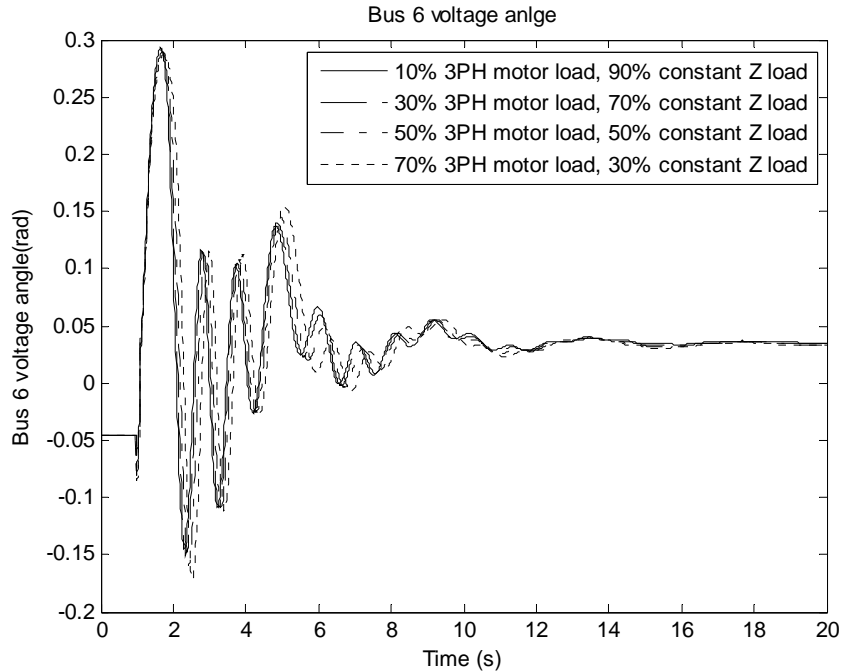settled to a new stable value.

Figure 6-4 Bus 6 voltage angle for three-phase motor load

6.3.2   Single-phase motor load

The tests in this section are to investigate the influence of single-phase motor load on the power system. The distribution system arrangement is shown in Figure 6-1. Four distribution systems were configured with all single-phase motors but with various percentages. The four load cases are summarized in Table 6.2. The equipment-level model for single-phase induction machine is based on the phasor model of Section **Error! Reference source not found.**. Furthermore different protection switch setups were configured for each load case for a total of eight variations of load on bus 6.

Table 6.2 Distribution systems with single-phase motor load

| Case number	Constant Z load (%)	Motor load (%)	Motor type	Number of motors
1	90	10	Single -phase	720
2	70	30	Single -phase	2160
3	50	50	Single -phase	3600
4	30	70	Single -phase	5040

6.3.2.1   Protection switch setup

To represent an actual RAC, TOL and UVL protection logic was included

in the phasor model. Two protection switch configurations are defined in this

research to represent extreme settings:

- **Protection switch setup 1**: The TOL open time set is longer that the

  simulation time, thus disabling TOL protection. The UVL threshold is

  set at a very low level of 0.4 p.u..

- **Protection switch setup 2**: The TOL switch of the RAC disconnects

  the RAC from the grid after a stall of 5 seconds or longer. The UVL

 threshold is set at 0.52 p.u..

6.3.2.2   Simulation results with protection switch setup 1

The load power on bus 6 is shown in Figure 6-5. The real and reactive

power draw significantly increases for the 50% motor load case. This is because

the single-phase motors in the distribution system stalled and thus consumed more

power than normal operation. The reactive power increase is much more than the

active power due to the low power factor of RAC motors under stall condition.
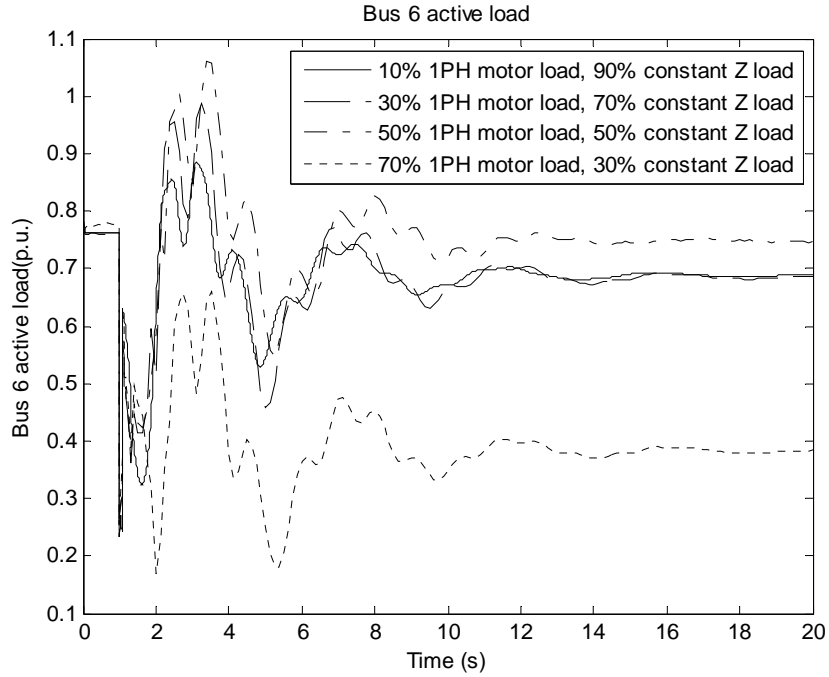
(a) Bus 6 load active power
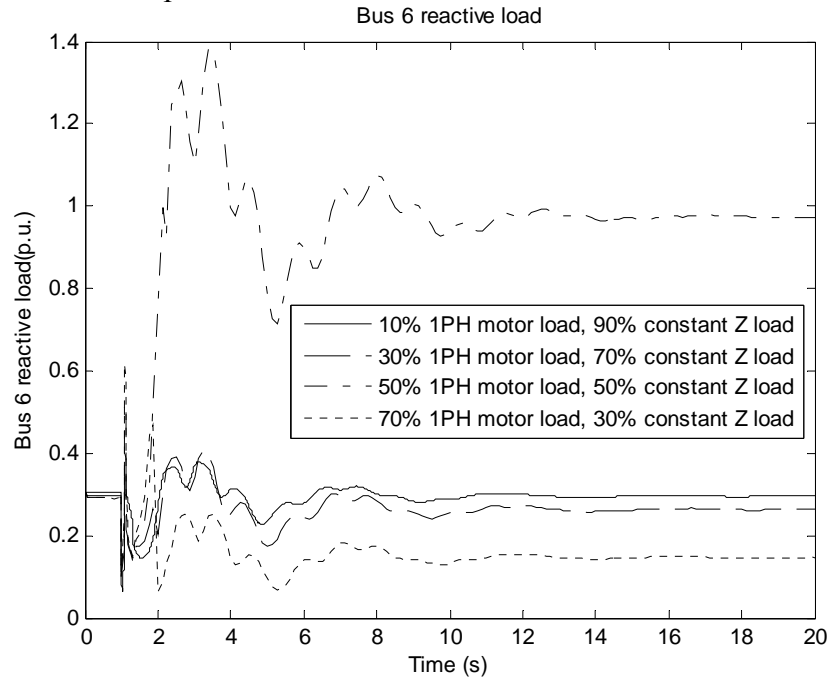
(b) Bus 6 load reactive power

Figure 6-5 Bus 6 load power with protection setup 1

63

Since motor load of the 70% case was removed at 1.9158 seconds by UVL

protection, the total load reduced significantly.

The voltages magnitude and angle at bus 6 are shown in Figure 6-6 and

Figure 6-7 respectively. The voltage magnitude and angle in all test cases reached
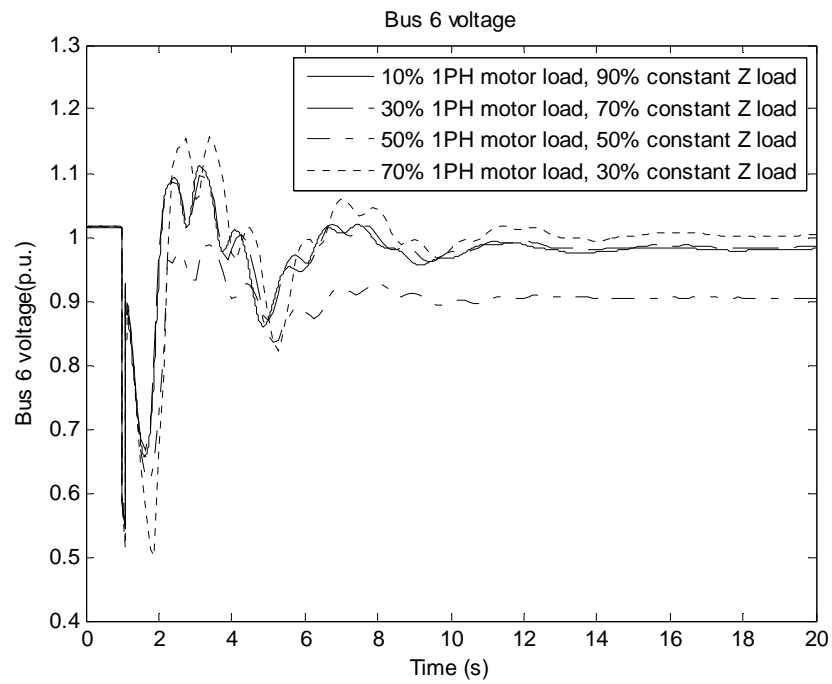
a stable level after the fault.

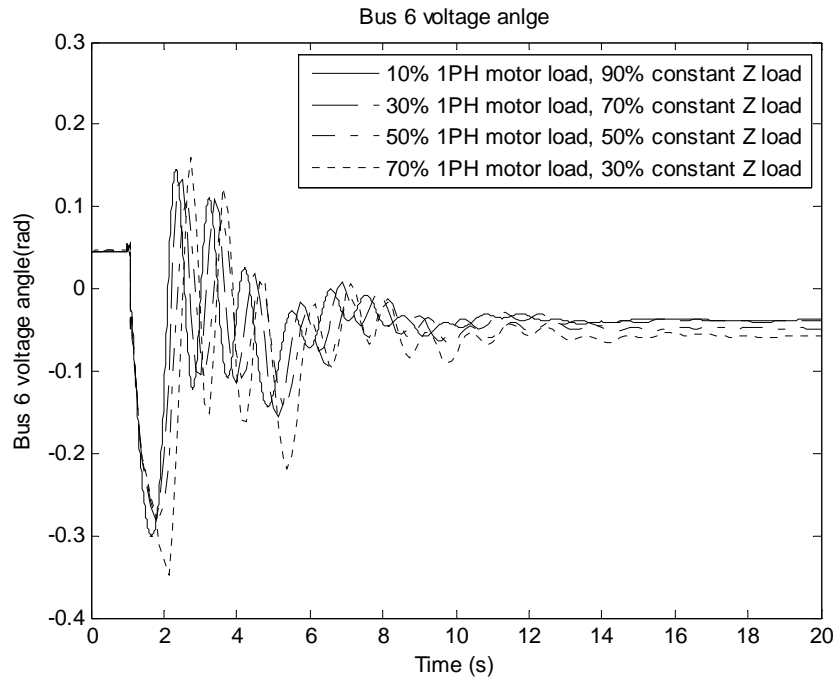Figure 6-6 Bus 6 voltage magnitude with protection setup 1

Figure 6-7 Bus 6 voltage angle with protection setup 1

In case that all the RAC motors included in the power system are equipped with protection setup 1, simulation results shows that:

- For 10 % motor load, the motor speed was almost constant during the entire simulation.

- For the 30% single-phase motor load, the speed reduced a little during the fault but recovered shortly after it was cleared.

- For the 50% single-phase motor case, the motors stalled at 2.005 seconds.

- For the 70% single-phase motor load case, the under-voltage contact switch opened at 1.9158 seconds

6.3.2.3   Simulation results with protection switch setup 2

The power at bus 6 during the simulation is shown in Figure 6-8.

Bus 6 active load

(a) Bus 6 load active power

Bus 6 reactive load
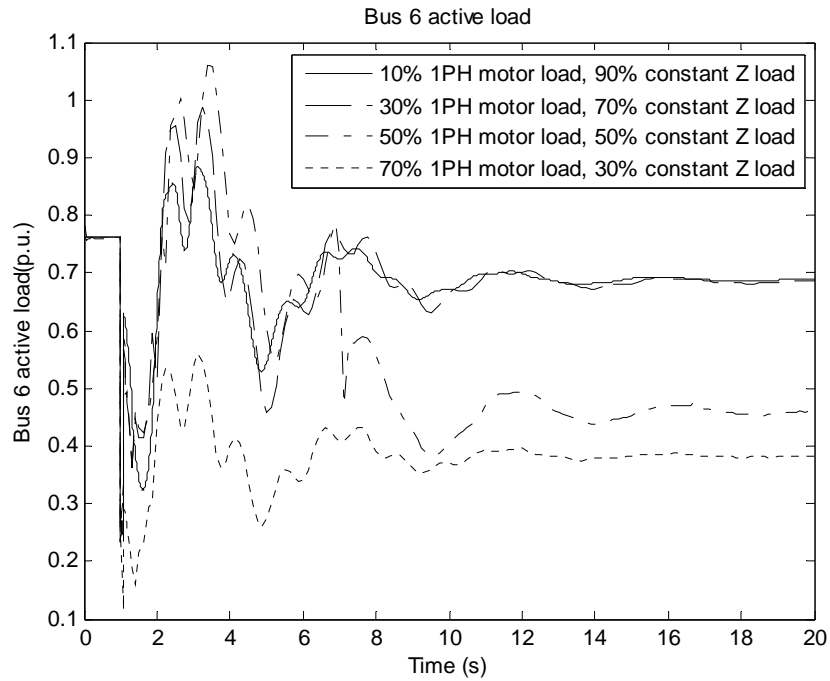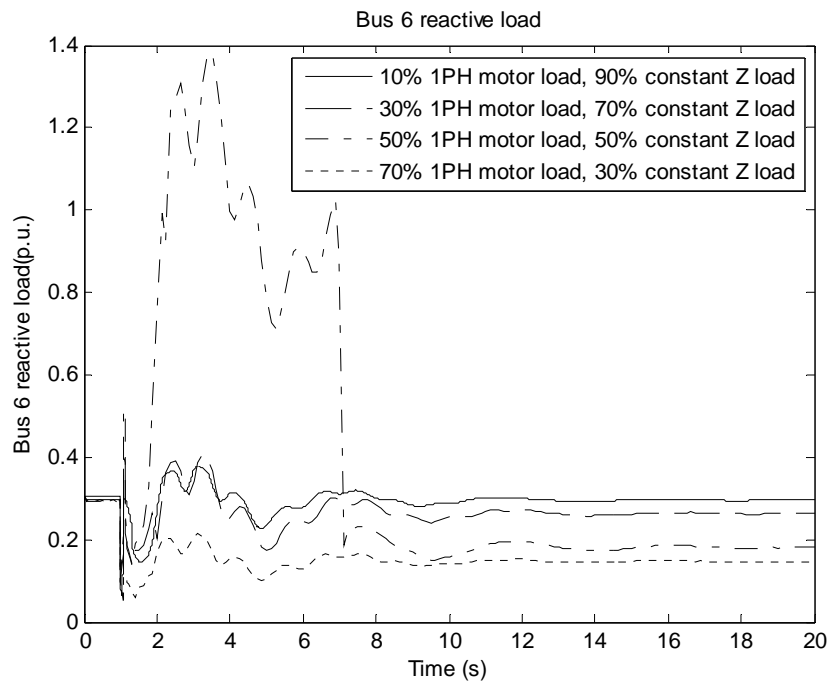
(b) Bus 6 load reactive power

Figure 6-8 Bus 6 load power with protection setup 2

Since the stalled motors of the 50% single-phase motor load case consume much

more power, the TOL switch removed the entire single-phase motor load at about 7

s. Load shedding can also be seen for the 70% single-phase motor load case.

Figure 6-9 shows after the fault was cleared, the bus voltage drop of the 50%

case is much lower than other 3 test cases. This is due to the high power demand

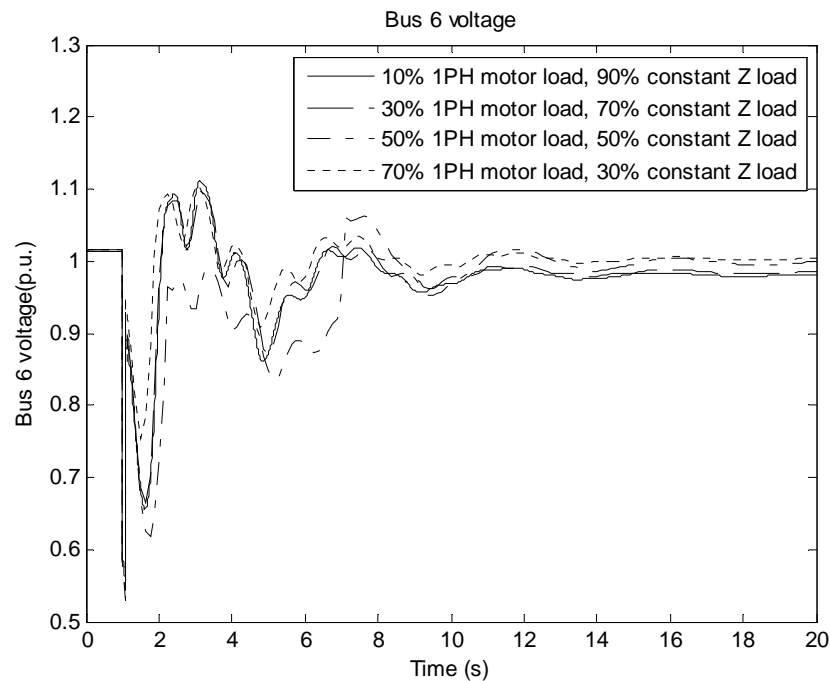of the stalled machines. After the motors are disconnected, the voltage recovers.

Figure 6-9 Bus 6 voltage magnitude with protection setup 2

The bus angles presented in Figure 6-10 show that power system is able to

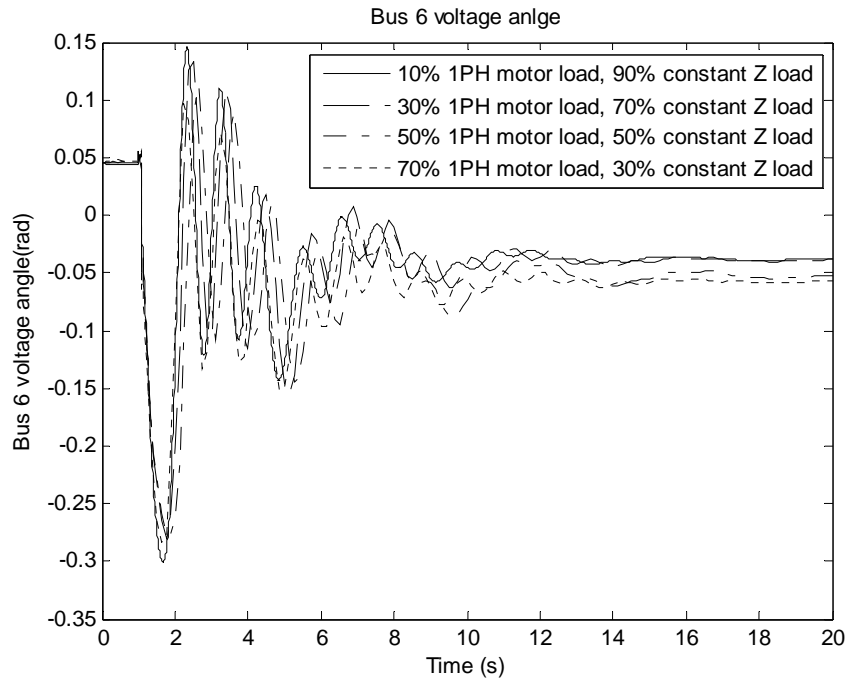keep the rotor angle stable with the protection switch setup 2.

Figure 6-10 Bus 6 voltage angle with protection setup 2

In the case that all RAC motors are equipped with the protection switch setup 2, results indicate:

- For the 10% single-phase motor load, neither protection mechanisms activated.

- Also for the 30% motor load case neither protection mechanisms activated.

- For the 50% motor load case the UVL switch did not open but the motor stalled at 2.005 s thus triggering the TOL switch 5 seconds later.

- For the 70% single-phase motor load, the UVL protection switch opened at 1.0395 s.

6.4   Case analysis

Simulation results from the previous section are now compared in a

different manner. Single phase and the equivalent three phase simulation results are compared for a given percentage of motor load penetration. Table 6.3 shows the various comparison sets.

Table 6.3 Comparison sets for different motor load percentage

Comparison set	Motor type	Protection switch setup
10% motor load	Three-phase	None
	Single-phase	Setup 1
	Single-phase	Setup 2
30% motor load	Three-phase	None
	Single-phase	Setup 1
	Single-phase	Setup 2
50% motor load	Three-phase	None
	Single-phase	Setup 1
	Single-phase	Protection switch setup 2
70% motor load	Three-phase	None
	Single-phase	Protection switch setup 1
	Single-phase	Protection switch setup 2

6.4.1   10% motor load

Figure 6-11 shows the bus apparent power and Figure 6-12 shows the bus voltage magnitude. It can be seen in Figure 6-11 that after the fault, the apparent power in the three and single-phase motor load cases have a slight difference. This is because of changes in power flow in the post-fault transmission network. The apparent power of the 10% single-phase motor load with switch setups 1 and 2 are the same because no switches opened in both cases. The voltage magnitudes

69

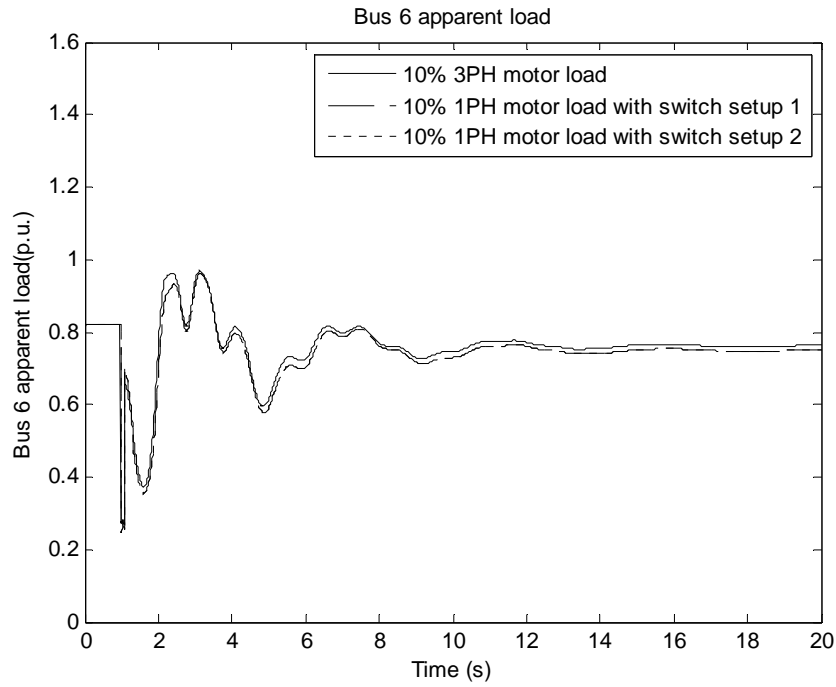in all the 10% cases are essentially identical.

Figure 6-11 Bus 6 load apparent power for 10% motor load

Figure 6-12 Bus 6 voltage magnitude for 10% motor load

6.4.2   30% motor load

Figure 6-13 shows the load bus apparent power and Figure 6-14 shows the

load bus voltage magnitude for 30% motor load case. The apparent power of the

30% single-phase motor load with switch setups 1 and 2 are the same because no

switches opened in both cases. The voltage magnitudes in all 30% motor load test

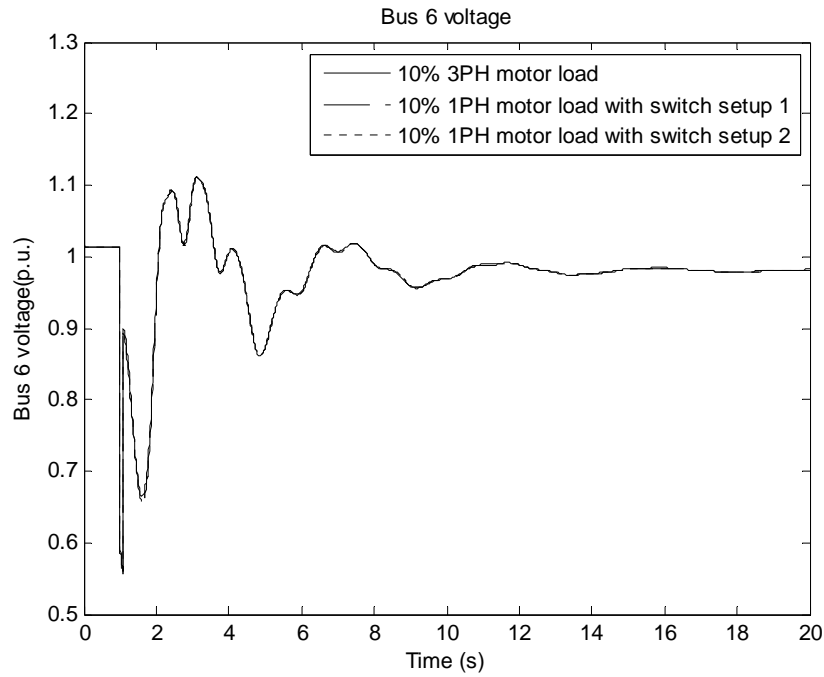cases nearly match each other.
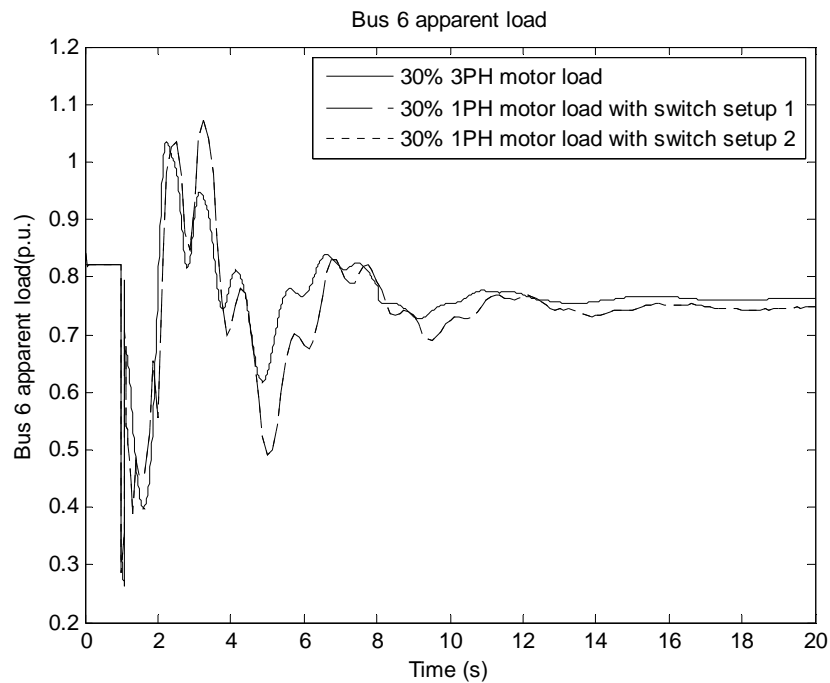
Figure 6-13 Bus 6 load for 30% motor load
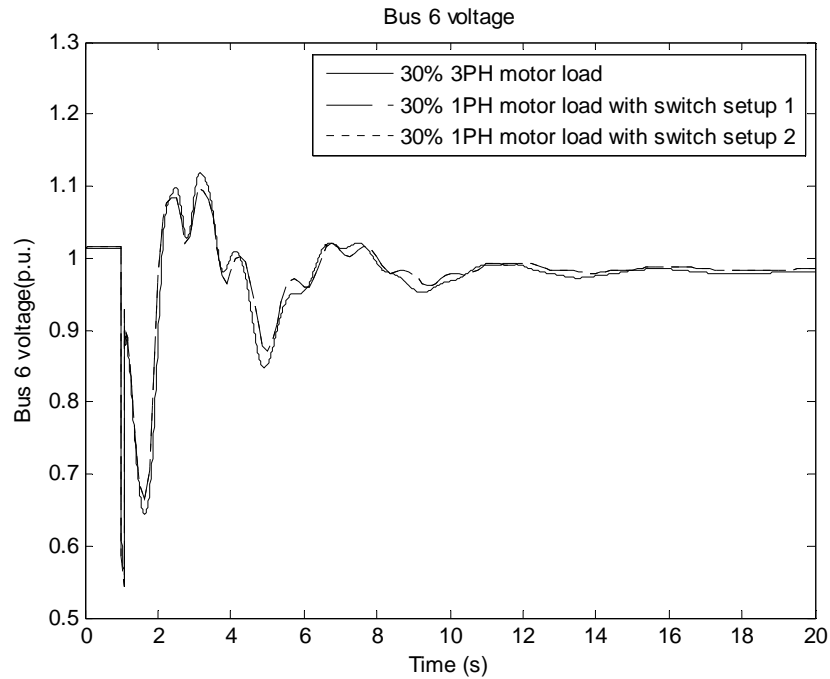
Figure 6-14 Bus 6 voltage magnitude for 30% motor load

6.4.3   50% motor load

Figure 6-15 shows the bus apparent power for the 50% motor load case.

The TOL switch opened at 7.005 s for the single-phase motor load with switch

setup 2. This removed the motors load from the distribution network. Differences

can be noted between the single phase motor models and equivalent three phase

motor approximation.
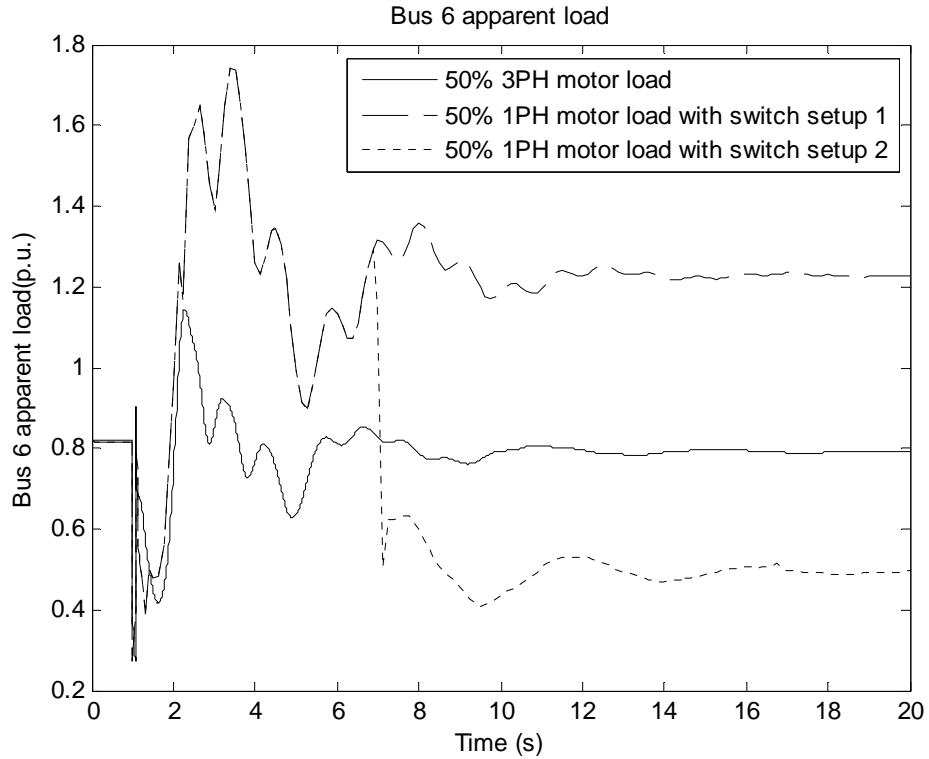
Figure 6-15 Bus 6 load for 50% motor load

Figure 6-16 shows the bus voltage magnitude for 50% motor load case.

With switch setup 2, the voltage increases after the TOL switch opens at 7.005 s.

Since the TOL switch did not open in 50% case with switch setup 1, the high

power demand pulled the voltage down. These two 50% single-phase motor cases

illustrate FIDVR. Again it can be seen that the three phase aggregate

approximation is not sufficiently accurate for this type of voltage stability study.
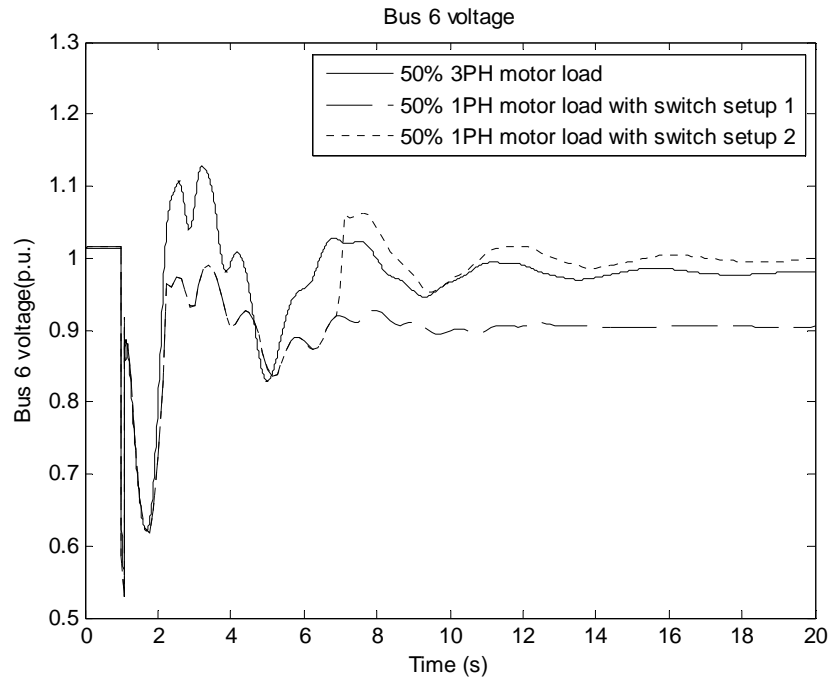
Figure 6-16 Bus 6 voltage magnitude for 50% motor load

6.4.4   70% motor load

Figure 6-17 shows the bus apparent power and Figure 6-18 shows the bus

voltage magnitude for 70 % motor load case. The three-phase motor load

recovered but the single-phase motor loads were removed soon after the fault,

both from UVL protection. The single phase motor load with protection setup 2

(.4 p.u. UVL threshold) experienced a deep voltage drop. Both single phase motor

load cases experienced greater voltage sag than the equivalent three phase case.

Figure 6-17 Bus 6 load for 70% motor load

Figure 6-18 Bus 6 voltage magnitude for 70% motor load

CHAPTER 7

CONCLUSIONS AND FUTURE WORK

7.1   Conclusions

In this work simulation of fault induced delayed voltage recovery was

investigated. The focus was primarily on load representation of residential air

conditioners in simulation.

First the topic of voltage stability was categorized. Static and dynamic

simulation methods were discussed in context of voltage stability. Voltage

stability indices were categorized. The FIDVR voltage stability phenomenon was

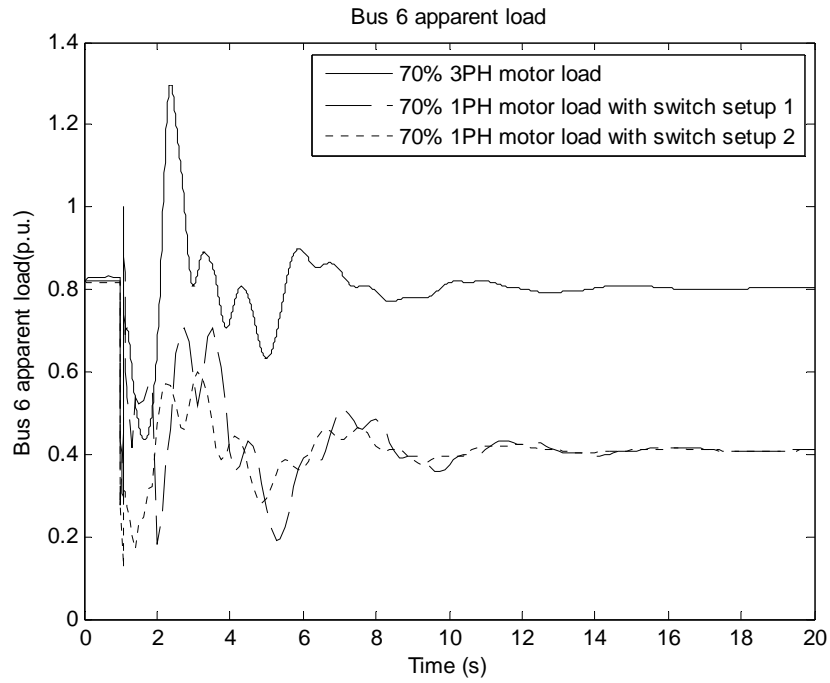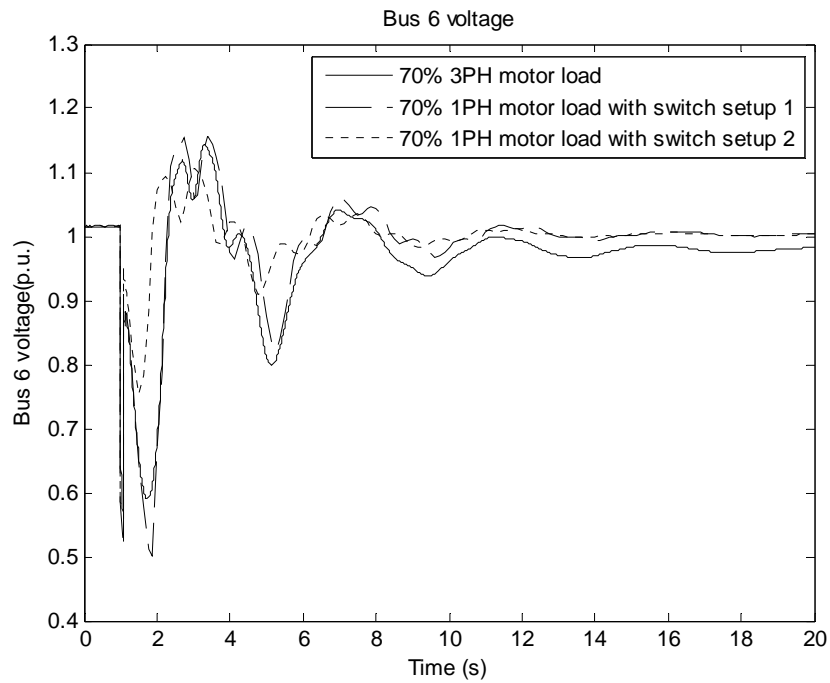defined and a brief literature review of various FIDVR events was presented. Also

some FIDVR solutions were listed.

Static load, dynamic load, and composite load modeling and associated

parameter extraction methods were presented. Common dynamic models for

single and three phase induction machines were listed.

Properties of typical RACs were then discussed. Stalling, protection

circuitry, and restarting characteristics of RACs were presented. Past work on

modeling of RACs in context of FIDVR was reviewed. Equipment level and grid

level modeling methods were discussed. The phasor model was presented as a

good equipment level model of RACs. Example three and single phase motor

models were tested for voltage sag characteristics in simulation.

A method was proposed to include detailed single phase load information

in a larger power system simulation to investigate the influence of motor load on

power system stability. An interface method for linking transmission network and

detailed distribution network in simulation was presented. The method entails passing data back and forth each time step.

A transmission network and several detailed distribution systems were built with different percentage motor load. Each single-phase motor in the distribution system was represented by the equipment-level phasor model, whose parameters were collected from a typical RAC compressor unit. Three-phase aggregate representations of RACs were also built in simulation with different percentage of motor load.

Simulations were conducted using the new interface method. A fault was set and cleared in an attempt to induce FIDVR. When the motor loads were represented by the three phase aggregate representation, no FIDVR events occurred. The same experiment was conducted with the detailed single phase models to represent the RACs. FIDVR was reproduced at 50 % motor load.

It can be concluded that the fault induced voltage sag in the distribution system becomes more severe with the increased single-phase motor load percentage. In these simulation experiments, the three-phase motor is able to represent the aggregation effect of the single-phase motor load only when the motor load percentage is 10% or 30%.

7.2   Future work

This work may be extended in a variety of directions. First more contingencies may be applied, such as unbalanced fault, generator outage, and increased system load. Also several more distribution systems with equipment-level models may be included to apply this new method to a larger area of the power system. A new grid-level single-phase motor model may be developed based on the findings from simulation results with a variety of contingencies. This new load model may provide a more accurate grid-level model representing the aggregating effect of the single-phase motor load.

REFERENCES

[1]   Prabha Kundur, *Power system stability and control*, New York: McGraw-Hill, 1994.

[2]   P. Kundur *et al.*, "Overview on definition and classification of power system stability," in *CIGRE/IEEE PES Int. Symp. on Quality and Security of Electric Power Delivery Systems*, 2003, pp. 1-4.

[3]   C. W. Taylor, *Power system voltage stability*, New York: McGraw-Hill, 1994.

[4]   *Appliance report on US households.* [Online]. Available: http://www.eia.doe.gov/emeu/reps/appli/all_tables.html

[5]   IEEE/PES power system stability subcommittee special publication, *Voltage stability assessment: concepts, practices and tools*, Aug., 2002.

[6]   J. D. Glover and M. S. Sarma, *Power System Analysis and Design*, Boston: PWS Pub., 1994.

[7]   L. M. C. Braz *et al.*, "A critical evaluation of step size optimization based load flow methods," *IEEE Trans. Power Syst.*, vol. 15, no. 1, pp. 202-207, Feb. 2000.

[8]   A. Wiszniewski, "New Criteria of Voltage Stability Margin for the Purpose of Load Shedding," *IEEE Trans. Power Del.*, vol. 22, no. 3, pp.1367-1371, Jul. 2007.

[9]   G. K. Morison *et al.*, "Voltage stability analysis using static and dynamic approaches," *IEEE Trans. Power Syst.*, vol.8, no. 3, pp. 1159-1171, Aug. 1993.

[10]   B. Delfino *et al.*, "Voltage stability of power systems: Links between static and dynamic approaches," *Electrotechnical Conference*, Bari, Italy, 1996, vol. 2, pp. 854-858.

[11]   M. Hasani and M. Parniani, "Method of combined static and dynamic analysis of voltage collapse in voltage stability assessment," *IEEE/PES Transmission and Distribution Conf. and Exhibition: Asia and Pacific*, 2005, pp.1-6.

[12]   IEEE special publication 90TH0358-2-PWR, Voltage stability of power systems: concepts, analytical tools, and industry experience, 1990.

[13]   I. Dobson, "An Iterative method to compute a closest saddle node or hope bifurcation instability in multidimensional parameter space," *1992 IEEE International Symposium on Circuits and Systems, ISCAS '92*. Proceedings, v. 5, pp. 2513 – 2516, 3-6 May 1992.

[14]   N. Flatabo *et al.*, "Voltage stability condition in a power transmission system calculated by sensitivity methods," *IEEE Trans. Power Syst.*, vol. 5, no. 4, pp. 1286-1293, Nov. 1990.

[15]   C. Lemaitre *et al.*, "An indicator of the risk of voltage profile instability for real-time control applications," *IEEE Trans. Power Syst.*, vol. 5, no. 1, pp. 154-161, 1990.

[16]   B. Gao *et al.*, "Voltage stability evaluation using modal analysis," *IEEE Trans. Power Syst.*, vol. 7, no. 4, pp. 1529-1542, Nov. 1992.

[17]   P. A. Lof *et al.*, "Fast calculation of a voltage stability index," *IEEE Trans. Power Syst.*, vol. 7, no. 1, pp. 54-64, Feb. 1992.

[18]   Voltage stability analysis program application guide, EPRI project RP3040-1, prepared by Ontario Hydro, October 1992.

[19]   C. A. Canizares *et al.*, "Comparison of performance indices for detection of proximity to voltage collapse," *IEEE Trans. Power Syst.*, vol. 11, no. 3, pp. 1441-1450, Aug. 1996.

[20]   A. Tiranuchit *et al.*, "Towards a computationally feasible on-line voltage instability index," *IEEE Trans. Power Syst.*, vol. 3, no. 2, pp.669-675, May 1988.

[21]   A.   Tiranuchit and R. J. Thomas, "A posturing strategy against voltage instabilities in electric power systems," *IEEE Trans. Power Syst.*, vol. 3, no. 1,   pp. 87-93, Feb. 1988.

[22]   H. Suzuki, "Study group 37 discussions, in *Proc. CIGRE 34th Session*, vol. 2, pp. 87-93, Feb. 1992.

[23]   Y. Tamura *et al.*, "Voltage instability proximity index (VIPI) based on multiple load flow solutions in ill-conditioned power systems," in *Proc. 27th IEEE Conf. on Decision and Control*, vol. 3, pp. 2114-2119, Dec. 1988.

[24]   J. Hasimoto *et al.*, "On the continuous monitoring of voltage stability margin in electric power systems," *Institute of Electrical Engineers of Japan Transaction*, vol. 108-B, no. 2, pp. 65-72, Feb. 1988. (In Japanese)

[25]   A. Takehara *et al.*, "Voltage stability preventive and emergency-preventive control using VIPI sensitivity," *Electrical Engineering in Japan*, vol. 143, no. 4, pp. 22-30, Jun. 2003.

[26]   P. Kessel and H. Glavitsch, "Estimating the voltage stability of a power system," *IEEE Trans. Power Del.*, vol. 1, no. 3, Jul. 1986.

[27]   T. Nagao, *et al.*, "Development of static and simulation programs for voltage stability studies of bulk power system,", *IEEE transactions on power systems*, v. 12,   Issue 1, pp. 273 – 281, Feb. 1997.

[28]   "Suggested techniques for voltage stability analysis," Technical report 93TH0620-5PWR, IEEE/PES, 1993.

[29]   NERC Transmission Issues Subcommittee and System Protection and Control Subcommittee, "A Technical Reference Paper Fault-Induced Delayed Voltage Recovery," Version 1.2, Jun. 2009.

[30]   B.R. Williams *et al.*, "Transmission voltage recovery delayed by stalled air-conditioner compressors," *IEEE Trans. Power Syst.*, vol. 7, no. 3, pp. 1173-1181, Aug. 1992.

[31]   J.W. Shaffer, "Air conditioner response to transmission faults," *IEEE Trans. Power Syst.*, vol. 12, no. 2, pp. 614-621, May 1997.

[32]   L. Taylor and S.M. Hsu, "Transmission voltage recovery following a fault event in the metro Atlanta area," *2000 IEEE PES Summer Meeting*, Seattle, WA, vol. 1, pp. 537-542, Jul. 2000.

[33]   P. Pourbeik and B. Agrawal, "A hybrid model for representing air-conditioner compressor motor behavior in power system studies," *2008 IEEE PES General Meeting - Conversion and Delivery of Electrical Energy in the 21st Century,* Pittsburgh, PA, pp. 1-8, Jul. 2008.

[34]   Lawrence Berkeley National Laboratory, "Final project report: load modeling transmission research," A California Institute for Energy and Environment (CIEE) Report, Mar. 2010.

[35]   IEEE Task Force on Load Representation for Dynamic Performance, "Load representation for dynamic performance analysis," *IEEE Trans. Power Syst.*, vol. 8, no. 2, pp. 472-482, May 1993.

[36]   J. Machowski, *et al.*, *Power system dynamics: stability and control*, 2nd ed., Wiley, 2008.

[37]   WECC Load Modeling Task Force, Load Modeling for Power System Studies [Online]. Available: http://www.nerc.com/docs/pc/tis/10_Load_Modeling_for_Power_System_Studies.pdf

[38]   Leonard L. Grigsby, *Electric power generation, transmission, and distribution*, 2nd ed., CRC Press, 2007.

[39]   W. W. Price, *et al.*, "Load modeling for power flow and transient stability computer studies," *IEEE Trans. Power Systems,* vol. 3, no. 1, pp. 180-187, Feb 1988.

[40]   G. Karady and K. Holbert, *Electrical energy conversion and transport: an interactive computer-based approach*, IEEE Computer Society Press, 2004.

[41]   M. N. Bandyopadhyay, *Electrical Machines: Theory and Practice*, Prentice-Hall of India Pvt.Ltd.,Oct. 30, 2008.

[42]   N. Mohan, *Advanced Electric Drives*, Minneapolis. MN: Mnpere, 2001.

[43]   D. W. Novotny and T. A. Lipo, *Vector Control and Dynamics of AC Drives*. New York: Oxford University Press, 1996.

[44]   C. M. Trout, Essentials of Electric Motors and Controls, Jones and Bartlett Publishers. LLC, 2010

[45]   R. Miller, M. Miller, *Industrial Electricity and Motor Controls*, McGraw-Hill Inc.,2008

[46]   B. Lesieutre *et al.*, "Phasor modeling approach for single phase A/C motors," *2008 IEEE PES General Meeting*, Pittsburgh, PA, pp. 1-7, Jul. 2008.

[47]   L. Y. Taylor *et al.*, "Development of load models for fault induced delayed voltage recovery dynamic studies," *2008 IEEE PES General Meeting - Conversion and Delivery of Electrical Energy in the 21st Century*, Pittsburgh, PA , pp. 1 - 7, 20-24 Jul. 2008

[48]   W. H. Kersting, *Distribution system modeling and analysis*, Taylor & Francis Group, LLC., 2007.

[49]   A. M. Gaikwad *et al.*, "Results of residential air conditioner testing in WECC," *2008 IEEE PES General Meeting - Conversion and Delivery of Electrical Energy in the 21st Century*, Pittsburgh, PA, pp. 1 – 9, Jul. 2008.

[50]   D. Kosterev *et al.*, "Load Modeling in Power System Studies: WECC Progress Update," *2008 IEEE PES General Meeting - Conversion and Delivery of Electrical Energy in the 21st Century*, Pittsburgh, PA, pp. 1-8, Jul. 2008.

[51] C. A. Baone *et al.*, "Local voltage support from distributed energy resources to prevent air conditioner motor stalling," *2010 Innovative Smart Grid Technologies (ISGT)*, pp. 1-6, 2010.

[52] V. Stewart and E. H. Camm, "Modeling of stalled motor loads for power system short-term voltage stability analysis," *2005 IEEE PES General Meeting*, San Francisco, CA, vol. 2, pp. 1887-1892, Jun. 2005.

[53] PSAT Reference Manual
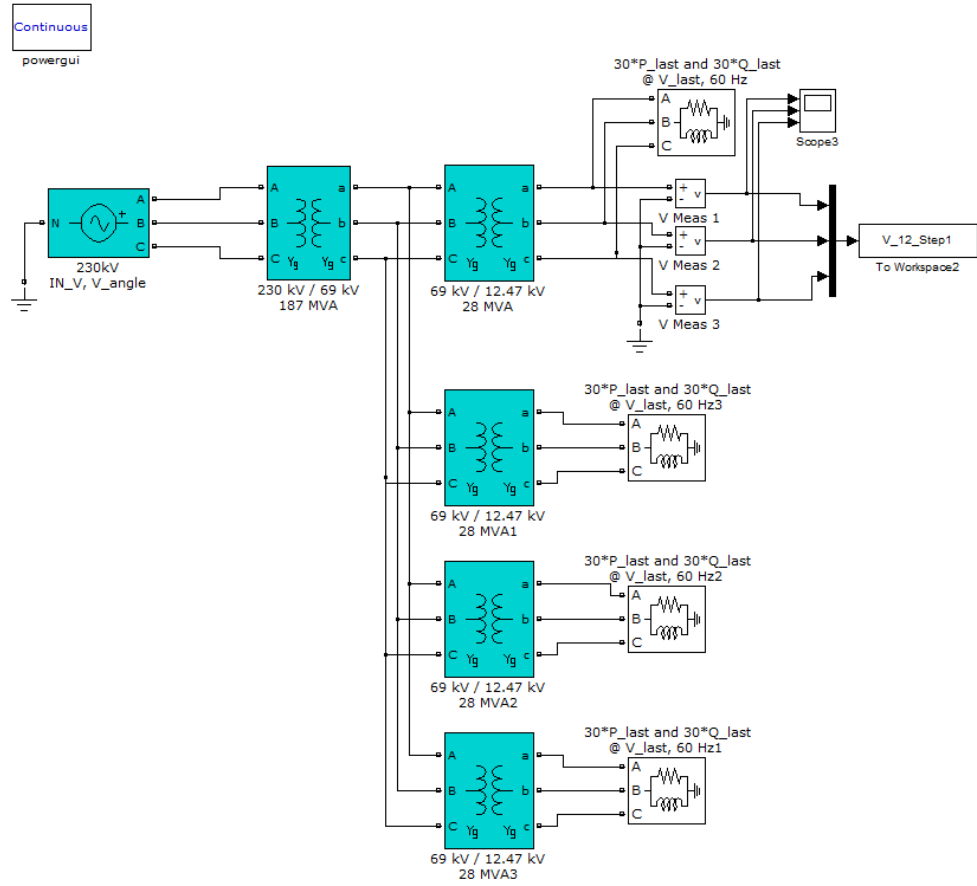
APPENDIX A

DISTRIBUTION SYSTEM SIMULATION

Figure A-1 Simulink step 1 for calculating end voltage after transformer
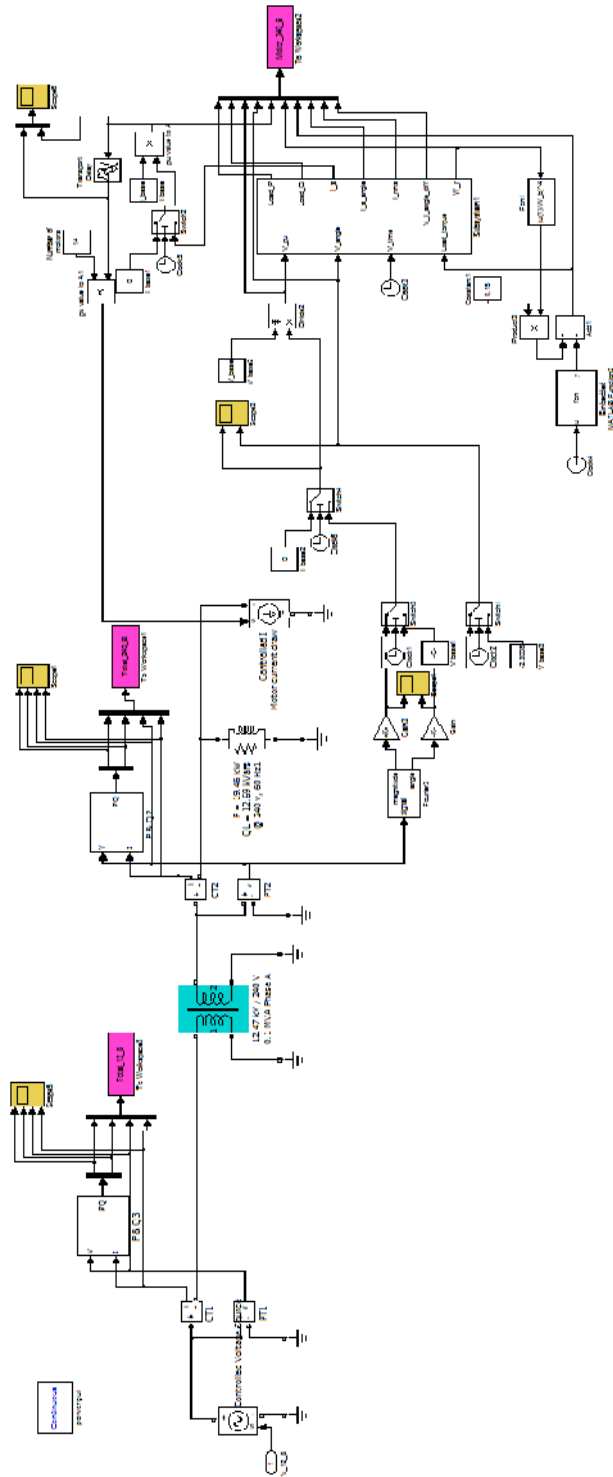
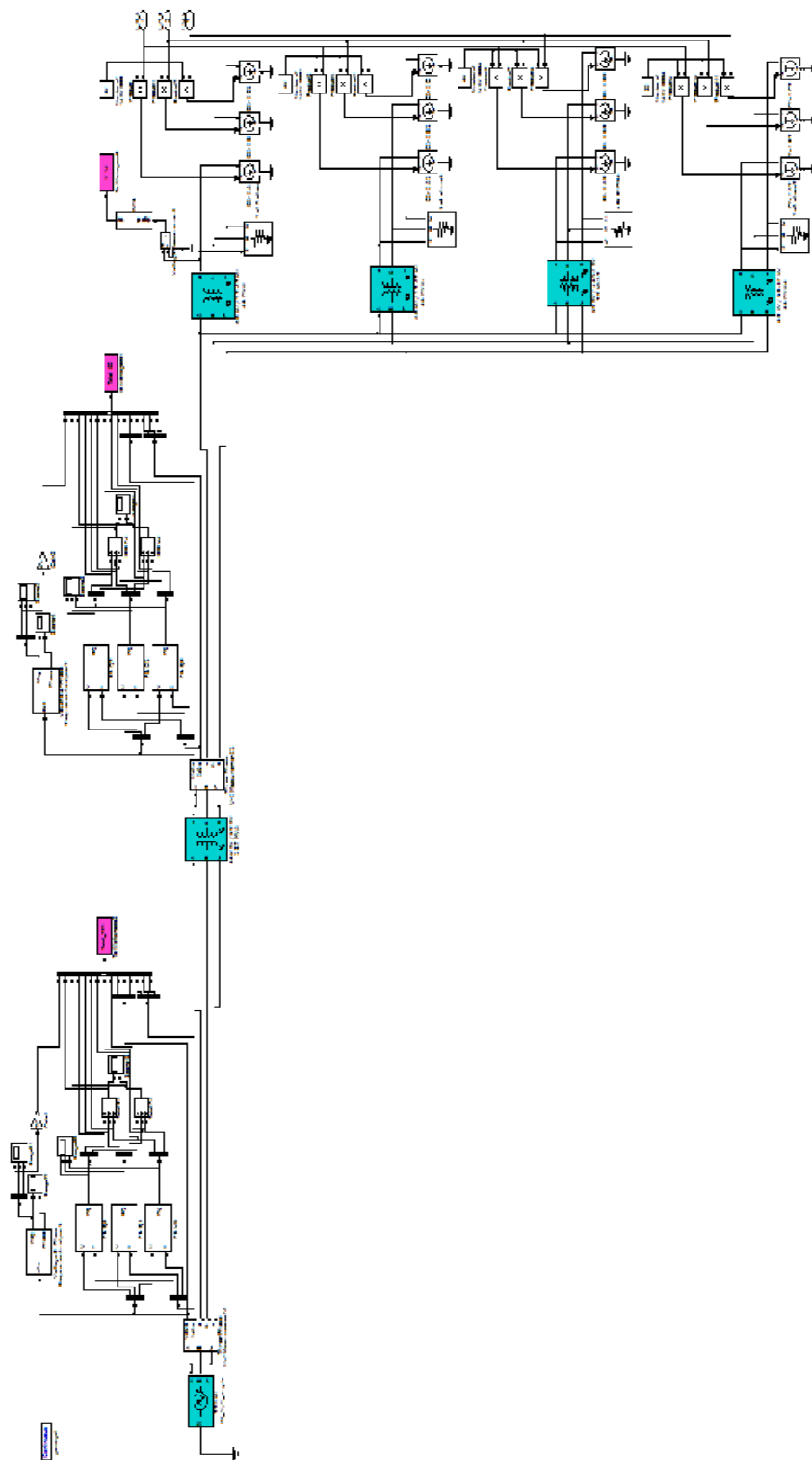Figure A-2 Simulink step 2 for calculating load on 69/12.47 transformer

Figure A-3 Simulink step 3 for calculating load applied transmission load bus

APPENDIX B

DATA EXCHANGE PROGRAM

A.1 Coding built in PSAT

```matlab
%Update P, Q, and V_p based on simulation from t0 to DAE.t
if T_last < DAE.t
    SimulinkStartTime=Settings.t0;
    % End time is increased by 1.5 s,which is the time duration for
    % 1PH motor to get its normal operation status
    SimulinkEndTime=DAE.t+1.5;
    %DAE.y(15)shows the bus 6 voltae magnitude during time-domain
    %simulation
    SimulinkVoltage=(DAE.y(15))*Bus.con(6,2)*1000;
    %DAE.y(6)shows the bus 6 voltae angle in rad during time-domain
    %simulation
    SimulinkAngle=DAE.y(6)*180/pi;
    %DAE.y(1)shows the bus 1 (swing bus) voltae angle in rad during
    %time-domain simulation
    Simulink_swing_Angle=DAE.y(1);
    %Call simulation in distribution network
    [p_local,q_local,V_p]=Local_simulink_connection(...
        SimulinkStartTime,...
        SimulinkEndTime,SimulinkVoltage,SimulinkAngle,...
        Simulink_swing_Angle,Simulink_PSAT_Step);
    T_last=DAE.t;
    %Update the P, Q, and V value of transmission load bus based on
    %simulation in Simulink
    %Update the bus 6 voltage
    DAE.y(15)=V_p;
    %Update the bus 6 load, if the applied load is out of acceptable
    %range, the applied load will be multiply with a factor to insure
    %the actural load applied on the bus 6 is the power needed by the
    %distribution network
    if DAE.y(15)<PQ.con(1,7)
        PQ.con(1,4)=p_local*DAE.y(15)^2/PQ.con(1,7)^2;
        PQ.con(1,5)=q_local*DAE.y(15)^2/PQ.con(1,7)^2;
    elseif DAE.y(15)>PQ.con(1,6)
        PQ.con(1,4)=p_local*DAE.y(15)^2/PQ.con(1,6)^2;
        PQ.con(1,5)=q_local*DAE.y(15)^2/PQ.con(1,6)^2;
    else
        PQ.con(1,4)=p_local;
        PQ.con(1,5)=q_local;
    end
%$$$$$$$$$$$$$$$$$$$$$$$$$$$$$$$$$$$$$$$$$$$$$$$$$$$$$$$$$$$$$$$$$$$$$$$$
$$$$$$
end
```

A.2 Coding for time-domain power flow analysis in Simulink

```matlab
function[p_local,q_local,V_p]=Local_simulink_connection(...
    SimulinkStartTime,SimulinkEndTime,SimulinkVoltage,...
    SimulinkAngle,Simulink_swing_Angle,Simulink_PSAT_Step)
%Record the system data during the entire simulation in Simulink
global Db_S_1 Db_S_2A Db_S_2B Db_S_2C Db_S_3_230 Db_S_3_69
%Record the simulation initial and final stage
global Simul_stage_1 Simul_stage_2A Simul_stage_2B
```

```matlab
global Simul_stage_2C Simul_stage_3
%Record exchange data between simulink and psat.
global Simulink_PSAT_Step
% Record the start and end time of simulation
global SimulinkStartTime SimulinkEndTime
%For parameters of RAC motor
global V_freq W_s W_b R_ds R_qs X_r X_c X_ds X_qs X_m H n
global A_sat b_sat T_o f_base V_base P_base I_base Z_base T_base
global X1 X2A X2B X2C X3
global IN_V V_angle
global V_12_Step1_R Total_12_A_R Total_12_B_R Total_12_C_R
global Db_last V_last P_last Q_last

%Update the input voltage of distribution system with bus 6 voltage
vector
IN_V=SimulinkVoltage;
V_angle=SimulinkAngle;
%Perform simulation step 1, get the voltage applied on the motor
[Data_row_last,Data_col_last]=size(Db_S_1);
open_system('HV_local_21_Step_1.mdl')
hAcs = getActiveConfigSet(gcs);
hAcs.set_param('StartTime', 'SimulinkStartTime');
hAcs.set_param('StopTime', 'SimulinkEndTime');
hAcs.set_param('LoadInitialState','on');
simOut = sim('HV_local_21_Step_1.mdl');
%%%%%
V_12_Step1_R=V_12_Step1;
[P_row,P_col]=size(V_12_Step1.time);
for row=1:P_row
    Db_S_1(row+Data_row_last,1)=V_12_Step1.time(row,1);
    Db_S_1(row+Data_row_last,2)=V_12_Step1.signals.values(row,1);
    Db_S_1(row+Data_row_last,3)=V_12_Step1.signals.values(row,2);
    Db_S_1(row+Data_row_last,4)=V_12_Step1.signals.values(row,3);
end
%Base on applied voltage, calculate the motor response in each phase
%Perform simulation step 2 for Phase A
[Data_row_last,Data_col_last]=size(Db_S_2A);
open_system('HV_local_21_Step_2_A.mdl')
hAcs = getActiveConfigSet(gcs);
hAcs.set_param('StartTime', 'SimulinkStartTime');
hAcs.set_param('StopTime', 'SimulinkEndTime');
hAcs.set_param('LoadInitialState','on');
simOut = sim('HV_local_21_Step_2_A.mdl');
%%%%%
Total_12_A_R=Total_12_A;
[P_row,P_col]=size(Motor_240_A.time);
for row=1:P_row
  Db_S_2A(row+Data_row_last,1)=Motor_240_A.time(row,1);
  Db_S_2A(row+Data_row_last,2)=Motor_240_A.signals.values(row,1);
  Db_S_2A(row+Data_row_last,3)=Motor_240_A.signals.values(row,2);
  Db_S_2A(row+Data_row_last,4)=Motor_240_A.signals.values(row,3);
  Db_S_2A(row+Data_row_last,5)=Motor_240_A.signals.values(row,4);
  Db_S_2A(row+Data_row_last,6)=Motor_240_A.signals.values(row,5);
  Db_S_2A(row+Data_row_last,7)=Motor_240_A.signals.values(row,6);
  Db_S_2A(row+Data_row_last,8)=Motor_240_A.signals.values(row,7);
```

```matlab
    Db_S_2A(row+Data_row_last,9)=Motor_240_A.signals.values(row,8);
    Db_S_2A(row+Data_row_last,10)=Motor_240_A.signals.values(row,9);
    Db_S_2A(row+Data_row_last,11)=Motor_240_A.signals.values(row,10)
    ;
    Db_S_2A(row+Data_row_last,12)=Total_240_A.signals.values(row,1);
    Db_S_2A(row+Data_row_last,13)=Total_240_A.signals.values(row,2);
    Db_S_2A(row+Data_row_last,14)=Total_240_A.signals.values(row,3);
    Db_S_2A(row+Data_row_last,15)=Total_240_A.signals.values(row,4);
    Db_S_2A(row+Data_row_last,16)=Total_12_A.signals.values(row,1);
    Db_S_2A(row+Data_row_last,17)=Total_12_A.signals.values(row,2);
    Db_S_2A(row+Data_row_last,18)=Total_12_A.signals.values(row,3);
    Db_S_2A(row+Data_row_last,19)=Total_12_A.signals.values(row,4);
end

%Perform simulation step 2 for Phase B
[Data_row_last,Data_col_last]=size(Db_S_2B);
open_system('HV_local_21_Step_2_B.mdl')
hAcs = getActiveConfigSet(gcs);
hAcs.set_param('StartTime', 'SimulinkStartTime');
hAcs.set_param('StopTime', 'SimulinkEndTime');
hAcs.set_param('LoadInitialState','on');
simOut = sim('HV_local_21_Step_2_B.mdl');
%%%%%%
Total_12_B_R=Total_12_B;
[P_row,P_col]=size(Motor_240_B.time);
for row=1:P_row
  Db_S_2B(row+Data_row_last,1)=Motor_240_B.time(row,1);
  Db_S_2B(row+Data_row_last,2)=Motor_240_B.signals.values(row,1);
  Db_S_2B(row+Data_row_last,3)=Motor_240_B.signals.values(row,2);
  Db_S_2B(row+Data_row_last,4)=Motor_240_B.signals.values(row,3);
  Db_S_2B(row+Data_row_last,5)=Motor_240_B.signals.values(row,4);
  Db_S_2B(row+Data_row_last,6)=Motor_240_B.signals.values(row,5);
  Db_S_2B(row+Data_row_last,7)=Motor_240_B.signals.values(row,6);
  Db_S_2B(row+Data_row_last,8)=Motor_240_B.signals.values(row,7);
  Db_S_2B(row+Data_row_last,9)=Motor_240_B.signals.values(row,8);
  Db_S_2B(row+Data_row_last,10)=Motor_240_B.signals.values(row,9);
  Db_S_2B(row+Data_row_last,11)=Motor_240_B.signals.values(row,10)
  ;
  Db_S_2B(row+Data_row_last,12)=Total_240_B.signals.values(row,1);
  Db_S_2B(row+Data_row_last,13)=Total_240_B.signals.values(row,2);
  Db_S_2B(row+Data_row_last,14)=Total_240_B.signals.values(row,3);
  Db_S_2B(row+Data_row_last,15)=Total_240_B.signals.values(row,4);
  Db_S_2B(row+Data_row_last,16)=Total_12_B.signals.values(row,1);
  Db_S_2B(row+Data_row_last,17)=Total_12_B.signals.values(row,2);
  Db_S_2B(row+Data_row_last,18)=Total_12_B.signals.values(row,3);
  Db_S_2B(row+Data_row_last,19)=Total_12_B.signals.values(row,4);
end

%Perform simulation step 2 for Phase C
[Data_row_last,Data_col_last]=size(Db_S_2C);
open_system('HV_local_21_Step_2_C.mdl')
hAcs = getActiveConfigSet(gcs);
hAcs.set_param('StartTime', 'SimulinkStartTime');
hAcs.set_param('StopTime', 'SimulinkEndTime');
hAcs.set_param('LoadInitialState','on');
```

```matlab
simOut = sim('HV_local_21_Step_2_C.mdl');
%%%%%
Total_12_C_R=Total_12_C;
[P_row,P_col]=size(Motor_240_C.time);
for row=1:P_row
  Db_S_2C(row+Data_row_last,1)=Motor_240_C.time(row,1);
  Db_S_2C(row+Data_row_last,2)=Motor_240_C.signals.values(row,1);
  Db_S_2C(row+Data_row_last,3)=Motor_240_C.signals.values(row,2);
  Db_S_2C(row+Data_row_last,4)=Motor_240_C.signals.values(row,3);
  Db_S_2C(row+Data_row_last,5)=Motor_240_C.signals.values(row,4);
  Db_S_2C(row+Data_row_last,6)=Motor_240_C.signals.values(row,5);
  Db_S_2C(row+Data_row_last,7)=Motor_240_C.signals.values(row,6);
  Db_S_2C(row+Data_row_last,8)=Motor_240_C.signals.values(row,7);
  Db_S_2C(row+Data_row_last,9)=Motor_240_C.signals.values(row,8);
  Db_S_2C(row+Data_row_last,10)=Motor_240_C.signals.values(row,9);
  Db_S_2C(row+Data_row_last,11)=Motor_240_C.signals.values(row,10)
  ;
  Db_S_2C(row+Data_row_last,12)=Total_240_C.signals.values(row,1);
  Db_S_2C(row+Data_row_last,13)=Total_240_C.signals.values(row,2);
  Db_S_2C(row+Data_row_last,14)=Total_240_C.signals.values(row,3);
  Db_S_2C(row+Data_row_last,15)=Total_240_C.signals.values(row,4);
  Db_S_2C(row+Data_row_last,16)=Total_12_C.signals.values(row,1);
  Db_S_2C(row+Data_row_last,17)=Total_12_C.signals.values(row,2);
  Db_S_2C(row+Data_row_last,18)=Total_12_C.signals.values(row,3);
  Db_S_2C(row+Data_row_last,19)=Total_12_C.signals.values(row,4);
end


%Perform simulation step 3 and calculate the latest P,Q, and V_P
[Data_row_last,Data_col_last]=size(Db_S_3_230);
open_system('HV_local_21_Step_3.mdl')
hAcs = getActiveConfigSet(gcs);
hAcs.set_param('StartTime', 'SimulinkStartTime');
hAcs.set_param('StopTime', 'SimulinkEndTime');
hAcs.set_param('LoadInitialState','on');
simOut = sim('HV_local_21_Step_3.mdl');
%Find load and V+
[P_row P_Col]=size(Total_230.signals.values);
for row=1:P_row
  Db_S_3_230(row+Data_row_last,1)=Total_230.time(row,1);
  Db_S_3_230(row+Data_row_last,2)=Total_230.signals.values(row,1);
  Db_S_3_230(row+Data_row_last,3)=Total_230.signals.values(row,2);
  Db_S_3_230(row+Data_row_last,4)=Total_230.signals.values(row,3);
  Db_S_3_230(row+Data_row_last,5)=Total_230.signals.values(row,4);
  Db_S_3_230(row+Data_row_last,6)=Total_230.signals.values(row,5);
  Db_S_3_230(row+Data_row_last,7)=Total_230.signals.values(row,6);
  Db_S_3_230(row+Data_row_last,8)=Total_230.signals.values(row,7);
  Db_S_3_230(row+Data_row_last,9)=Total_230.signals.values(row,8);
  Db_S_3_230(row+Data_row_last,10)=Total_230.signals.values(row,9)
  ;
  Db_S_3_230(row+Data_row_last,11)=Total_230.signals.values(row,10
  );
  Db_S_3_230(row+Data_row_last,12)=Total_230.signals.values(row,11
  );
  Db_S_3_230(row+Data_row_last,13)=Total_230.signals.values(row,12
  );
```

```matlab
    Db_S_3_230(row+Data_row_last,14)=Total_230.signals.values(row,13
    );
    Db_S_3_230(row+Data_row_last,15)=Total_230.signals.values(row,14
    );
    Db_S_3_230(row+Data_row_last,16)=Total_230.signals.values(row,15
    );
end
for row=1:P_row
    Db_S_3_69(row+Data_row_last,1)=Total_69.time(row,1);
    Db_S_3_69(row+Data_row_last,2)=Total_69.signals.values(row,1);
    Db_S_3_69(row+Data_row_last,3)=Total_69.signals.values(row,2);
    Db_S_3_69(row+Data_row_last,4)=Total_69.signals.values(row,3);
    Db_S_3_69(row+Data_row_last,5)=Total_69.signals.values(row,4);
    Db_S_3_69(row+Data_row_last,6)=Total_69.signals.values(row,5);
    Db_S_3_69(row+Data_row_last,7)=Total_69.signals.values(row,6);
    Db_S_3_69(row+Data_row_last,8)=Total_69.signals.values(row,7);
    Db_S_3_69(row+Data_row_last,9)=Total_69.signals.values(row,8);
    Db_S_3_69(row+Data_row_last,10)=Total_69.signals.values(row,9);
    Db_S_3_69(row+Data_row_last,11)=Total_69.signals.values(row,10);
    Db_S_3_69(row+Data_row_last,12)=Total_69.signals.values(row,11);
    Db_S_3_69(row+Data_row_last,13)=Total_69.signals.values(row,12);
    Db_S_3_69(row+Data_row_last,14)=Total_69.signals.values(row,13);
    Db_S_3_69(row+Data_row_last,15)=Total_69.signals.values(row,14);
    Db_S_3_69(row+Data_row_last,16)=Total_69.signals.values(row,15);
end
%%%%%%%%%%%%%%%%%%%%%%%%%%%%%%%%%%%%%%%%%%%%%%%%%%%%%%%%%%%%%%%%%%%%
%Find the latest P,Q, and V_P and return these value to the function
[Data_row_last,Data_col_last]=size(Db_S_3_230);
V_p_230=Db_S_3_230(Data_row_last,2);
P_230=Db_S_3_230(Data_row_last,3);
Q_230=Db_S_3_230(Data_row_last,4);
%If positive sequence of supply voltage in distribution system is more
%than input voltage, then update the transmission load bus voltage
if V_p_230 > SimulinkVoltage
    V_p=V_p_230/230000;
else
    V_p=SimulinkVoltage/230000;
end
%Assume there are two same local netowork
p_local=2*P_230/1e8;
q_local=2*Q_230/1e8;

%Write data to Simulink_PSAT_Step
[Simu_row,Simu_col]=size(Simulink_PSAT_Step);
Simulink_PSAT_Step(Simu_row+1,1)=SimulinkStartTime;%s
Simulink_PSAT_Step(Simu_row+1,2)=SimulinkEndTime-1.5;%s
Simulink_PSAT_Step(Simu_row+1,3)=SimulinkVoltage/230000;%p.u.
Simulink_PSAT_Step(Simu_row+1,4)=SimulinkAngle*pi/180;%rad
Simulink_PSAT_Step(Simu_row+1,5)=Simulink_swing_Angle;%rad
Simulink_PSAT_Step(Simu_row+1,6)=V_p;%p.u.
Simulink_PSAT_Step(Simu_row+1,7)=p_local;%p.u.
Simulink_PSAT_Step(Simu_row+1,8)=q_local;%p.u.
```